1-28-2015

Radiation Study of the Organic Photovoltaic Cell P3HT:PCBM

Camron Kouhestani

Camron G Kouhestani
Candidate

Electrical and Computer Engineering
Department

This thesis is approved, and it is acceptable in quality and form for publication:

Approved by the Thesis Committee:

Dr. Ganesh Balakrishnan , Chairperson

Dr. Christos G. Christodoulou

Dr. Roderick A. B. Devine

Dr. Kenneth E. Kambour

RADIATION STUDY OF THE ORGANIC PHOTOVOLTAIC CELL P3HT:PCBM

by

CAMRON G KOUHESTANI

BACHELOR'S OF SCIENCE
ELECTRICAL ENGINEERING

THESIS

Submitted in Partial Fulfillment of the Requirements for the Degree of

Master of Science
Electrical Engineering

The University of New Mexico
Albuquerque, New Mexico

December 2014

Dedication

I would like to dedicate this to my family. Without their love and support, I would not have achieved what I have today. Without their guidance, I would not have the motivation to follow through with this degree.

I would also like to dedicate this work to my coworkers Dr. Roderick A. B. Devine, Dr. Kenneth E. Kambour, and Mr. Duc D. Nguyen for their guidance, patience, support and wisdom throughout the latter half of my undergraduate career and my graduate career at the University of New Mexico.

Acknowledgement

I would first like to acknowledge Dr. Roderick A. B. Devine for his guidance, support, and his assistance with experimental set-up and conceptual understanding.

I would like to acknowledge Dr. Kenneth E. Kambour for his guidance, support, and his assistance with the simulations and conceptual understanding

I would like to thank Mr. Duc D. Nguyen for all his support as a coworker and friend throughout our time at Air Force Research Labs (AFRL).

I would also like to thank Mr. Clay Mayberry and Mr. Craig Kief for the opportunities they presented me during my undergraduate career that paved the way to my graduate career.

I would like to thank Dr. Harold P. Hjalmarson, Dr. John Grey, Mr. Alan Thomas, Mr. David Manley, Mr. William Kemp, and Mr. Richard Netzer for the conversations and guidance throughout my graduate career.

I would like to thank Dr. Gang Li, Professor Yang Yang and Professor Yang Yang's group at University of California at Los Angeles (UCLA) for the fabrication of these devices as well as helpful conversations to progress understanding the fundamentals of these devices.

I would also like to thank my committee members: Dr. Ganesh Balakrishnan, Dr. Christos Cristodoulou, Dr. Roderick A. B. Devine, and Dr. Kenneth E. Kambour.

The work performed in this thesis was sponsored by the Air Force Research Laboratory under agreement number FA9453-08-2-0259 and also partially funded by the AFSOR through AFOSR-09RV01COR.

Radiation Study of the Organic Photovoltaic Cell P3HT:PCBM

By
Camron G Kouhestani

B.S., Electrical Engineering, University of New Mexico, 2013
M.S., Electrical Engineering, University of New Mexico, 2014

Abstract

The need for inexpensive, dependable, radiation hard solar cells for use in space applications has led to attention being focused on organic semiconductor based solar cells. Such cells are lightweight, flexible and are potentially useful in conformal coverage applications. While these solar cells are less efficient (presently < 12%) than traditional silicon or III-V semiconductor based solar cells, the reduced efficiency is compensated for by their lower weight. This leads to a higher specific power and hence a lower load for launch. Furthermore, their flexibility is a particularly positive attribute since this renders them less vulnerable to vibration damage during the launch process. It must also be added that since one envisages solution processing deposition of the organic cells on very large area sheets (roll by roll technology) one can then also imagine a scenario in which a chosen panel area can be simply tailored from a large roll, thereby speeding up the process of solar panel production. Before this somewhat futuristic approach to low power solar panel production can become a reality for space applications, a full evaluation/understanding of their behavior in a radiation environment is necessary.

In this work, a detailed study has been performed on the archetypal organic photovoltaic poly(3-hexylthiophene) (6,6)-phenyl-C_{61}-butyric acid methyl ester (P3HT:PCBM). The interest of the applicability of organic photo-cells for use in space

based solar panels is derived from the recognition that “unusual” conditions exist which are not generally addressed by the organic photo-cell community. The defense presentation will cover the findings of pre-irradiation, irradiation, and post-irradiation characteristics; determination of the physical mechanisms resulting in the dominant photo-carrier loss mechanism, and a detailed investigation of the radiation effects.

Transient photo-voltage (TPV) measurements were utilized to evaluate carrier relaxation times in P3HT:PCBM based photo-cells over a wide range of open circuit voltages. Satisfactory agreement is found with data obtained by low frequency impedance measurements. This data set offers valuable insight into the loss mechanism to help material scientists develop new material that will have better power conversion efficiency. Furthermore, the results are promising for the development OPV technology for space based applications. We find that the experimental data is inconsistent with the theoretical behavior expected based on the generally accepted Langevin recombination model. In particular, the Langevin coefficient is three orders of magnitude smaller than the theoretical one and appears to be dependent on the carrier density. For the low light levels, the relaxation time variation is determined by the RC time constant behavior of the photodiode.

Table of Contents

List of Figures

1 Chapter 1 – Introduction

There is in general an increasing interest in researching renewable energy resources and photovoltaic solar cells, which utilize sunlight, access what is to all extents and purposes, the most abundant renewable energy source available. Our planet receives ~1.2×10^{17} W of solar energy, which one can usefully compare with the current rate of consumption, which is ~10,000 times smaller at ~1.3×10^{13} W. Solar energy alone, then, has the capacity to meet all the planet's energy needs for the foreseeable future. No other renewable energy sources have such a capacity, so they can only serve as auxiliary supplies in our future energy mix [1, 2].

1.1 Background to the Thesis

The solar energy industry has been dominated by inorganic materials, which are expensive to manufacture, and heavy. They can provide relatively high energy conversion efficiencies (~43% [3]), which may compensate for their shortfalls elsewhere. A relatively new class of solar cells (albeit of lower efficiency < 12% [4] see Fig. 1.1) is entering the industrial arena and these are made of organic semiconductor materials. They have a relatively simpler manufacturing process and include cheaper materials. If one concentrates on specific power (W/kg) (Fig. 1.4) [5] as a criterion, these lightweight materials already out perform advanced inorganics. Furthermore, as "plastics" they are significantly more flexible than their inorganic counterparts. We will therefore concentrate in the following on the mode of operation and properties of organic material based photovoltaic cells.

1.1.1 Organic Versus Inorganic Photovoltaics

1.1.1.1 Materials

In this work, I have made measurements using the active blended layer of poly(3-hexylthiophene) (P3HT) and (6,6)-phenyl-C_{61}-butyric acid methyl ester (PCBM) in a 1:1 weight ratio concentration. P3HT:PCBM is known to achieve photo-conversion efficiencies greater than 4% [6] and is studied as the "archetypical" organic photocell system.

1.1.1.2 Power Conversion Efficiency

The power conversion efficiency is the most commonly used parameter to compare the performance of one solar cell to another. Power conversion efficiency is defined as the ratio of energy output from the solar cell to input energy from the Sun (see Eq. 1.1 below). The efficiency of a solar cell depends upon the optical spectrum and intensity of the incident sunlight and therefore its black body temperature as well as the optical absorption spectrum of the cell itself. Standardized testing conditions for efficiency measurements are usually performed in a controlled manner in order to compare the performance from one device to another [7]. The equation for power conversion efficiency is [7]:

$$\eta = \frac{V_{oc} * I_{sc} * FF}{P_{in}} \qquad (1.1)$$

Where, η is the efficiency, V_{oc} is the open circuit voltage, I_{sc} is the short circuit current, FF is the fill factor and P_{in} is the power input from the Sun.

The best inorganic power conversion efficiencies are up to ~44.4% [7] – see Fig. 1.1, whilst the best organic cell conversion efficiency so far is about 12% [8]. The inorganic high efficiency is obtained using a triple junction of III-V type materials

absorbing at different wavelengths of the solar spectrum [9]. In contrast to the multi-junction inorganic photovoltaics (IPV), the higher organic photovoltaic material (OPV) efficiency is achieved by a single material. It is possible to achieve higher power conversion efficiencies by building OPVs in tandem like multi-junction IPVs [8].

In order to utilize the Sun more efficiently with a broad optical absorption band, the choice of material for the active layer in organic photovoltaic cells is critical. For this reason, many low band gap materials have been developed and improved in the past decade [6]. For polymers the band gap is dictated by the separation in energy of the highest occupied molecular orbitals (HOMO) of the n-type material and lowest unoccupied molecular orbitals (LUMO) levels of the p-type semiconductor. In inorganic solids these correspond to conduction and valence bands, respectively [10]. Unlike inorganic photo-cells where one usually considers the generation of electron-hole pairs, which then drift to their respective electrodes [10, 13], in organics one initially generates bound excitons [6, 10]. These diffuse to the donor/acceptor interface and are separated by the semiconductor built-in potential [6, 10] giving rise to free electron-hole pairs. In order to obtain efficient charge separation, the HOMO/ LUMO levels of the donor material should be 0.2-0.3 eV higher than the acceptor material, respectively. If the offset of these levels is too big, there is significant energy loss and to minimize this, the materials are chosen accordingly.

In IPV cells, holes and electrons are generated together, in the same phase of the material, and the photo-induced chemical potential gradient tends to drive them in the same direction. In addition, the built-in electric potential of inorganic devices drives the separation and flow of holes and electrons [11, 12].

In contrast, for the OPV, the excitons dissociate at interfaces, such as electrodes or, as in the case of heterojunction devices, at the interface between donor and acceptor organic materials [11]. So, the hole is generated in the donor phase and the electron is generated in the acceptor phase. As a consequence of the free carriers being spatially separated and existing in different phases, the photo-induced chemical potential drives them in opposite directions [11, 12].

This generation of charge carriers exists in different phases for two reasons: the first reason is the dielectric constant of the organic phase is usually low compared to inorganic semiconductors. The attractive Coulomb potential well around the initial electron-hole pair extends over a greater volume than it does in inorganic semiconductors [13]. Secondly, the non-covalent electronic interactions between organic molecules are weak compared to the inorganic semiconductor materials like silicon. The electron's wave function is spatially restricted, which allows it to be localized in the potential well of its conjugate hole (and vice versa) [13].

1.1.1.3 Carrier Type

Because the OPVs have low equilibrium carrier densities, excitonic solar cells under illumination are almost always majority carrier devices, unlike most IPV cells which are minority carrier devices [13]. The energy of a thermalized exciton is less than the energy of a free electron-hole pair; the difference being the exciton binding energy [13]. The diffusion of the minority carriers in the built-in electric potential creates the current for the inorganic devices. On the other hand, organic cells are majority carriers because holes exist primarily in the donor phase, electrons exist primarily in the acceptor phase, and the movements of these charges result directly in current flow [10, 11].

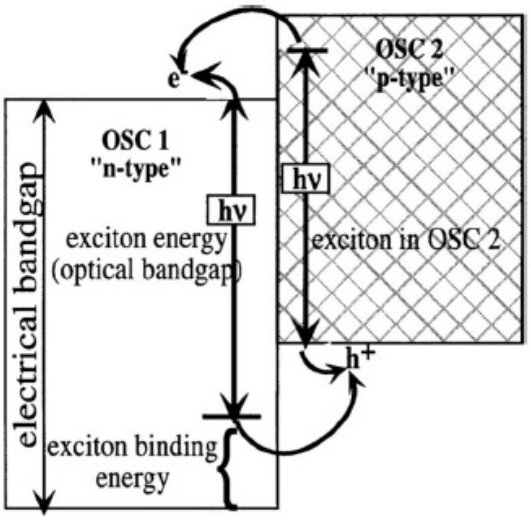

Figure 1.1. Energy-level diagram for an excitonic solar cell with no band bending but a band offset. Excitons created by light absorption in both organic semiconductors 1 and 2 do not possess enough energy to dissociate in the bulk ~except at trap sites. But the band offset between OSC1 and OSC2 provides an exothermic pathway for dissociation of excitons in both phases, producing electrons in OSC1 already separated from holes in OSC2. The band offset must be greater than the exciton binding energy for dissociation to occur [13].

The charge transport mechanisms that drive charged carriers towards the electrodes differ between inorganic and organic solar cells, Fig.1.2 . Photon absorption in IPV cells produces electron and hole pairs in the same material in the same phase and same spatial distribution. Because of the same spatial distribution for the two carrier types, the driving force for the transport by diffusion is identical and therefore, the electrons and holes are driven in the same direction [11, 12]. Diffusion is a small driving force in IPV cells and therefore, the electrical potential gradient present at the interface of a p-n junction is able to separate the photo-induced electrons from the holes efficiently. In an OPV, the charge transfer electrons and holes are in close proximity and therefore there is a large chemical potential gradient that drives the charge carriers away from the exciton dissociating interface [12].

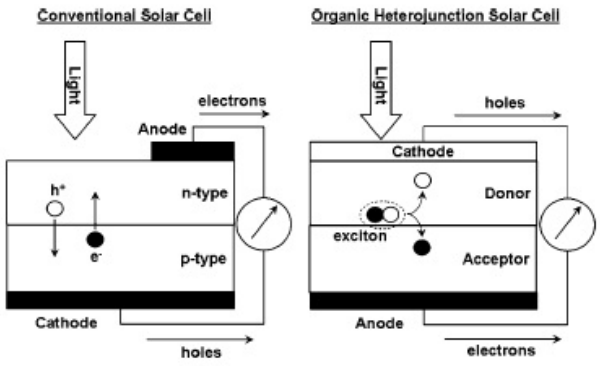

Figure 1.2. Schematic diagrams of a conventional p–n junction solar cell (left) and an organic heterojunction solar cell (right). The diagram highlights differences in carrier generation between the two types of devices [11].

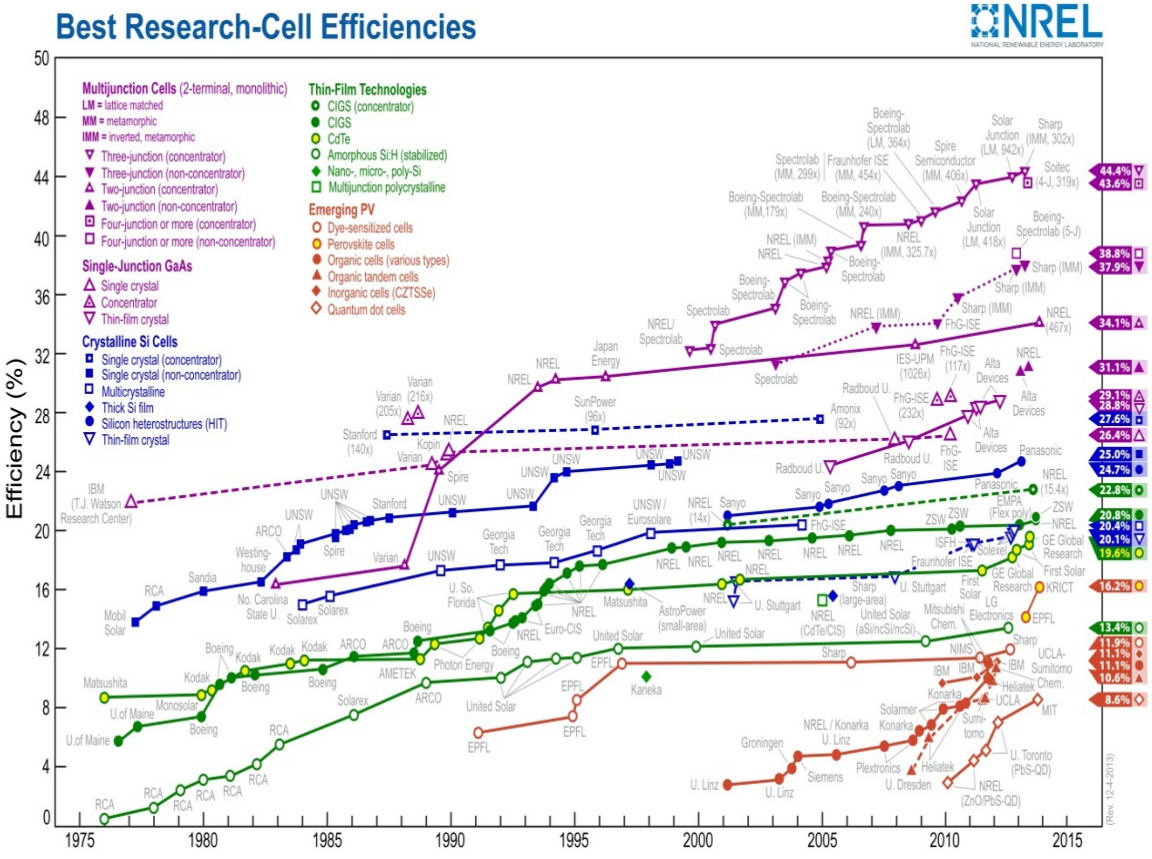

Figure 1.3. A graph of the evolution of power conversion efficiency between inorganic (purple, blue, and green) and organic (red) based photocells [3].

1.1.2 Solar Cell Applications in Space

Solar power generation using inorganic photocells is already used for both terrestrial and extraterrestrial applications. Note, on the positive side, in space, approximately 30% more watts/m^2 are available outside the atmosphere; However, there are different considerations that must be addressed with extraterrestrial usage that are not a problem for terrestrial applications. In particular, one must take into account the existence of different types of radiation in space.

There are a wide range of applications for extraterrestrial missions. Satellites and the International Space Station are the primary users today as well as the rovers that are exploring Mars. Traditional solar panels for spaced based operations are made of inorganic materials with power conversion efficiencies of ≥20% [14]. Research is being carried out on inorganics with potentially much higher efficiencies. There are many considerations that must be taken into account for solar panels in these environments that include radiation sensitivity, weight, solar power conversion efficiency, flexibility, price, etc., which will be described in the next section in more detail.

1.1.3 Advantages of OPV

The primary interest in organic photovoltaic cells derives from the promise of a relatively easy fabrication process [11]. In addition to easier fabrication, this new class of materials has a potential of providing environmentally safe, flexible, lightweight and inexpensive power generation [12].

Organic materials, when the efficiency is increased, will exhibit the advantages of nearly unlimited variability and low fabrication costs [15]. The cost reduction of organic photovoltaic fabrication results from the ease of processing from solutions. It can be

employed on a roll by roll basis. Furthermore, solution processing requires soluble polymers, which are also lower in cost than their inorganic counterpart [12]. Recent developments in ink-jet printing, micro-contact printing, and other soft lithography techniques have further improved low cost fabrication of large area integrated organic photovoltaic devices on both rigid and flexible substrates [12, 13, 16].

Since launch weight is a crucial factor for space based solar panels, specific power (power generated to weight ratio) is an increasingly more important parameter. For organic solar cells, the active layer is typically 100 nm thick to absorb 1/e photons [12] and because it only needs such a small thickness, less material is required thus reducing the array weight. Organic Solar cells and some thin film inorganics have made a giant leap in terms of this parameter with an unprecedented specific power value of 10W/g [16].

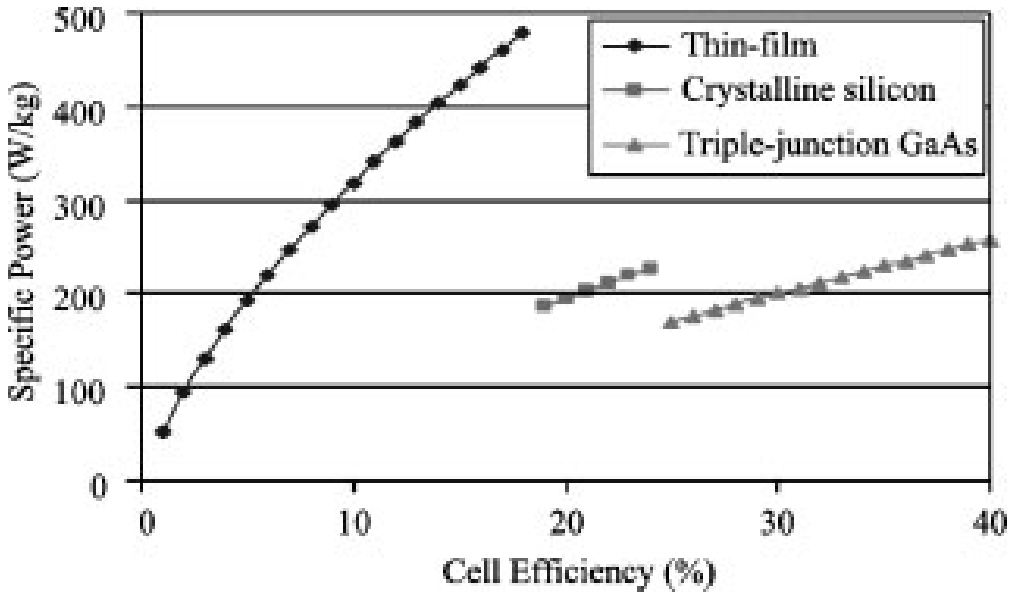

Figure 1.4. A graph of specific power comparison between thin-film organic photovoltaics and inorganic photovoltaics [5]

1.1.3.1 Potential Extraterrestrial Applications

OPV technology has never been used in space, but it is becoming a potential candidate to replace the IPV technology for specific applications.

IPVs are difficult to manufacture, heavy, fragile and expensive. It costs ~ $22,000 to put one kilogram of payload into space [17]. This is where specific power will come into account. Furthermore, IPVs are in general crystalline materials, which are not flexible and have low stress tolerances before cracking occurs. They may therefore be very sensitive to vibration during launch. Since OPVs can be built on a flexible substrate, they have a better chance of surviving these vibrations. The OPV specific power is significantly higher than the IPVs, which will reduce the cost of launch significantly.

1.1.4 Radiation Effects

Space based solar panels are subject to damaging radiation. There are seven basic terminologies that are necessary to understand radiation effects. These terminologies include: gamma rays, x-rays, alpha particles, beta particles, neutrons, protons and heavy ions.

1.1.4.1 Definitions

Gamma rays and x-rays are short-wave-length forms of electromagnetic radiation. A gamma ray has its origin in nuclear interaction, whereas an x-ray originates from stimulation of electrons in atomic levels by charged species (electrons) followed by relaxation and photon emission. The ways in which these photons interact with matter are similar. They are ionizing as well as highly penetrating and leave no remnant nuclear activity in the material irradiated [18]. In general they are not considered to be sources of displacement damage [18].

Alpha particles are the nuclei of helium atoms. They have a mass of 4 and a positive charge of 2 units. In space they normally have high kinetic energy (in the MeV range) and they interact strongly with matter and are both heavily ionizing and capable of atomic displacement damage. These particles have low penetrating power and travel in straight lines. A typical alpha particle of energy 5 MeV has a range of 50 mm in air and 23 μm in silicon [18].

Beta particles have the same mass as an electron, but may be either negatively or positively charged. With their small size and charge they penetrate matter more easily than alpha particles, but are more easily deflected. Their high velocity, normally approaching that of light, means they are lightly ionizing [18].

A neutron has the same mass as a proton but has no charge and consequently is difficult to stop. The neutron can be slowed down by hydrogenous material. Water is an especially effective shield for neutrons [18]. The capture of a neutron can result in the emission of a gamma ray after undergoing a transformation with a target species. Neutrons are classified according to their energy: thermal (<1eV); intermediate; and fast (>100keV). The proton is the nucleus of a hydrogen atom and carries a charge of 1 unit. The proton has a mass some 1800 times that of an electron, and consequently is more difficult to deflect, with a typical range of several centimeters in air and tens of micrometers in aluminum, at energies in the MeV range [18].

1.1.4.2 Units

The SI unit of energy is the joule (J), however, the electron volt (eV) is more frequently used in radiation technology. One eV is the energy gained by one electron in accelerating through a potential difference of 1 volt. The conversion factor is: 1eV =

$1.6*10^{-19}$ J. Energies in nuclear reactions are usually quoted in MeV or keV. A traditional unit of energy is the erg, (10^{-7} J) [18].

The rad and gray (Gy) are universal units of ionizing energy deposition; a rad has been absorbed by the sample of interest when 100 ergs/gram of energy has been deposited, and a gray when 1 joule per kilogram has been deposited. One rad thus equals 10^{-2} gray. Even though the gray is the SI unit, the rad is used because this is still the working unit for most published papers in radiation effects and also for current medical practice [18].

1.1.4.3 Radiation environment

The space radiation environment is composed of a variety of highly energetic particles with a wide range of energies. These particles are either trapped by one of the Earth's magnetic fields or are passing through the solar system [18].

The main elements of the radiation environment are:

1. Trapped radiation.
2. Cosmic rays.
3. Solar flares.

Space is pervaded by electron and proton plasmas with energies up to ~100 keV [18]. Within the radiation belts these particles represent the low-energy extremes of the trapped electron and proton populations (Fig. 1.5). In the outer zones of the magnetosphere, these particles are associated with the solar wind, and considerable fluxes will be encountered at very high altitudes. The low-energy particles are easily stopped by thin layers of material and hence only the outer-most surfaces such as thermal control material and solar cell cover slips are affected. The low energy plasma can cause

spacecraft charging, and the internal electronics may be affected by this charging and subsequent discharging [18].

1.1.4.3.1 The radiation belts

The Earth's radiation belts consist mainly of electrons and protons with high energy, which are trapped in the Earth's magnetic field. The field is similar to that of a magnetic dipole and in those regions where the field lines are closed; charged particles become trapped in the magnetosphere. The field is not geographically symmetrical; local distortions are caused by an offset and tilt of the magnetic axis and by geological influences. The Sun also heavily influences the magnetosphere by distorting it. The resulting form of the field has characteristics comparable to the wake of a solid object moving through a fluid. [18]

The electron environment consists of particles up to 7 MeV with the most energetic particles occurring in the outer zone. In contrast, proton energies extend to several hundred MeV, with the most energetic particles found at lower altitudes. The electron environment shows two flux maxima, referred to as the inner and outer zones. The inner zone extends from about 0.11 to 2.4 Earth radii (R_e) and the outer zone from 2.8 to 12 R_e. The gap between 2.5 and 2.8 R_e is referred to as the slot [18].

The proton environment does not exhibit inner and outer zones like the electron environment, the protons are found only in the inner zone. A 'cross-section' of the radiation belts is represented in Fig. 1.5, which shows the radial flux profiles in an equatorial orbit [18].

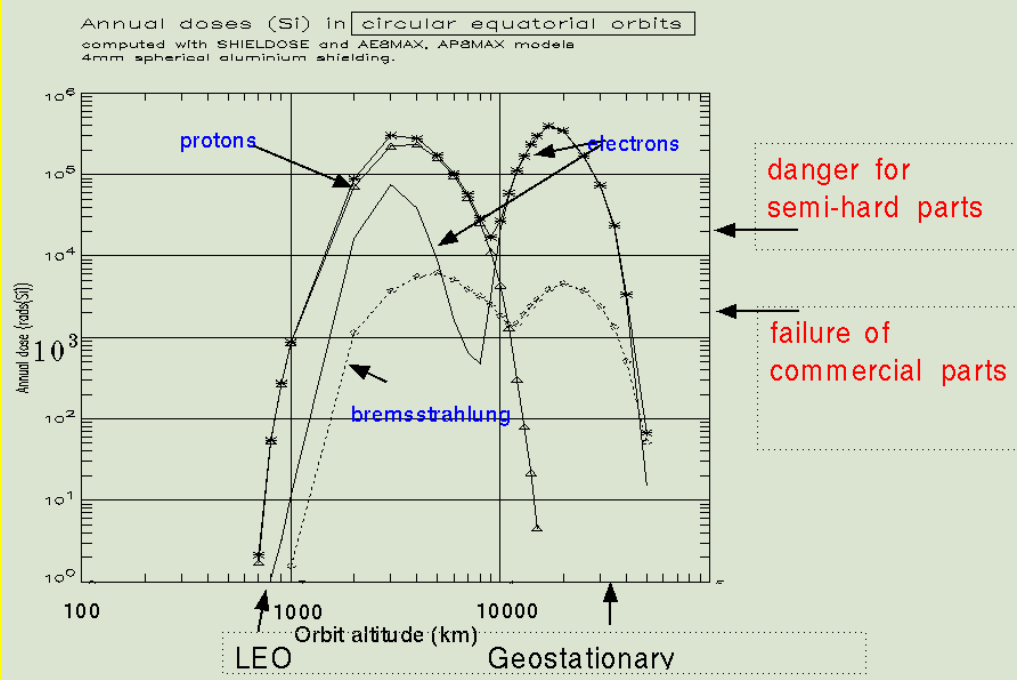

Figure 1.5. A plot of radiation dose as a function of altitude [19].

As mentioned previously, energetic electrons and protons lose their energy via ionizing radiation interaction with target materials. We therefore anticipate that satellites in or around low Earth orbits (Fig. 1.5) will be subjected to radiation of an ionizing nature.

1.1.4.3.2 Cosmic rays

There are three sources of cosmic rays: galactic, solar, and terrestrial. Galactic cosmic rays are primary cosmic rays, which originate outside the solar system but are associated with the galaxy. They provide a continuous, low-flux component of the radiation environment. The composition of galactic cosmic rays is about 85% protons, 14% alpha particles, and 1% heavier nuclei with energies extending to 1 GeV [18].

Terrestrial cosmic rays are the primary cosmic radiation which penetrates the Earth's atmosphere and is rapidly transformed by interactions which produce a cascade of

secondary radiation. These cascades take place in the main body of the atmosphere and the secondary rays produced at the earth's surface [18].

1.2 Thesis Objective

The work performed in this thesis was carried out in the context of a close collaboration with the research group of Professor Yang Yang of the Department of Materials Science, UCLA. The primary objective was, and remains, to develop efficient, rad hard OPVs that could be employed in space. On the basis of the text above, we developed a set of objectives for this thesis. Initially to familiarize ourselves with optimized measurement techniques and data interpretation methodology for OPV technology. Upon development of optimized experimental procedures, to study the physics in P3HT:PCBM active layer for 1:1 weight ratio only. In particular, to experimentally derive parameters of the OPV such as photo-carrier relaxation times, carrier density, and current-voltage data. There is still significant debate over the exact nature of the carrier relaxation process in OPVs and this must be addressed before one can reasonably extend our understanding to the effects of radiation. Finally, following an in-depth study of cell behavior, irradiation studies will be performed in an effort to understand the effects of radiation with the view to ultimately predicting the potential lifetime of these cells in the space environment. Since low earth orbital radiation (Fig. 1.5) is primarily due to the ionization component associated with electrons and protons these studies are particularly adapted to being performed in a research lab environment using either X-ray or ^{60}Co γ sources.

1.3 References for Chapter 1

[1] Unknown. (2006). Renewable Energy. California Energy Commission. Retrieved 24 October 2013 from http://www.consumerenergycenter.org/renewables/index.html

[2] Tao, M. (2008). Inorganic photovoltaic solar cells: silicon and beyond. *The Electrochemical Society Interface*, *17*(4), 30-35.

[3] Green, M. A., Emery, K., Hishikawa, Y., Warta, W., & Dunlop, E. D. (2012). Solar cell efficiency tables (version 39). *Progress in photovoltaics: research and applications*, *20*(1), 12-20.

[4] Li, G., Zhu, R., & Yang, Y. (2012). Polymer solar cells. *Nature Photonics*, *6*(3), 153-161.

[5] 2009 AFOSR/NRL Organic Review

[6] Hou, J., & Guo, X. (2013). Active Layer Materials for Organic Solar Cells. In *Organic Solar Cells* (pp. 17-42). Springer London.

[7] Honsberg, C., & Bowden, S. (2010). Retrieved 24 October 2013 from pveducation.org.

[8] Tanner, D., Mei, F., Sullivan, J., Choi, G., Koran, F., & Gold, M. P. Large area thin film solar module lamination. *pv-tech. org*.

[9] Stan, M., Aiken, D., Cho, B., Cornfeld, A., Diaz, J., Korostyshevsky, A, & Varghese, T. (2008, May). Evolution of the high efficiency triple junction solar cell for space power. In *Photovoltaic Specialists Conference, 2008. PVSC'08. 33rd IEEE* (pp. 1-6). IEEE.

[10] Kumar, A., Sista, S., & Yang, Y. (2009). Dipole induced anomalous S-shape< equation> IV</equation> curves in polymer solar cells. *Journal of Applied Physics*, *105*(9), 094512-094512.

[11] Benanti, T. L., & Venkataraman, D. (2006). Organic solar cells: An overview focusing on active layer morphology. *Photosynthesis research*, *87*(1), 73-81.

[12] T. Savenije, *ORGANIC SOLAR CELLS*. Delft University of Technology.

[13] Gregg, B. A., & Hanna, M. C. (2003). Comparing organic to inorganic photovoltaic cells: Theory, experiment, and simulation. *Journal of Applied Physics*, *93*(6), 3605-3614.

[14] Kumar, A., Devine, R., Mayberry, C., Lei, B., Li, G., & Yang, Y. (2010). Origin of Radiation-Induced Degradation in Polymer Solar Cells. *Advanced Functional Materials*, *20*(16), 2729-2736.

[15] Wöhrle, D., & Meissner, D. (1991). Organic solar cells. *Advanced Materials*, *3*(3), 129-138.

[16] Kaltenbrunner, M., White, M. S., Głowacki, E. D., Sekitani, T., Someya, T., Sariciftci, N. S., & Bauer, S. (2012). Ultrathin and lightweight organic solar cells with high flexibility. *Nature communications*, *3*, 770.

[17] Dave Drachlis. (unknown). Advanced Space Transportation Program: Paving the Highway to Space. Retrieved 24 October 2013 from http://www.nasa.gov/centers/marshall/news/background/facts/astp.html_prt.htm

[18] Holmes-Siedle, A., & Adams, L. (1993). Handbook of radiation effects.

[19] Daly, E. J., Drolshagen, G., Hilgers, A., & Evans, H. D. R. (1996, December). Space Environment Analysis: Experience and Trends. In *Environment Modeling for Space-Based Applications* (Vol. 392, p. 15).

2 Chapter 2 – Organic Photovoltaics

2.1 Physics, Chemistry, Engineering Background

2.1.1 Fabrication

All of the experiments were performed on devices fabricated by Prof. Yang Yang and Dr. Gang Li's group at the UCLA. A brief review of the fabrication technique is discussed in this section, which was pioneered by Gang Li et al. [1]. The primary layout of the organic solar cell from the bottom to top is as follows. The bottom of the device consists of a glass substrate coated with a transparent conductive oxide (TCO), [2, 3] typically Indium Tin Oxide (ITO), which is the anode. A conducting surface modifier layer which consists of polyethylenedioxythiophene: polystyrenesulphonate PEDOT:PSS is deposited on the anode. The active layer contains a blend of two types of organic materials [1], the electron donor material and an electron acceptor material. In one case these materials could be poly(3-hexylthiophene) (P3HT), which is the donor, and (6,6)-phenyl-C_{61}-butyric acid methyl ester (PCBM), which is the acceptor [1, 4]. The cathode layer comprises a thin layer of Calcium capped with Aluminum contacts. A quartz cover slide was epoxied onto the top to help protect the film against humidity and oxygen thereby slowing down the oxidization of the Calcium layer [1]. Fig. 2.1 shows the device layout.

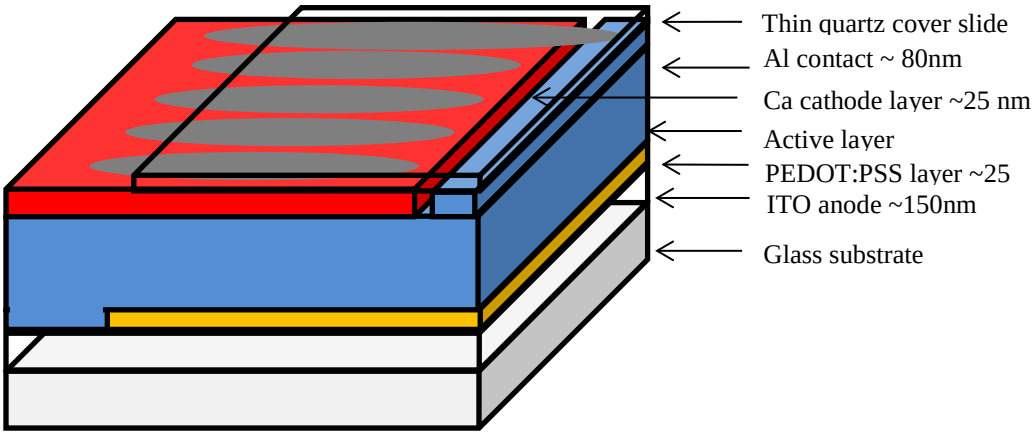

Figure 2.1. Construction of the organic solar cell. Note that the P3HT:PCBM concentrations are 1:1 by weight.

2.1.2 Operation

To create a functional photovoltaic cell, the two photoactive donor/acceptor materials are sandwiched together between two metallic electrodes. One electrode is transparent in order to allow photons to access the active layer. The other electrode doesn't have to be transparent and therefore is typically Aluminum. The electrodes collect the photo-generated charges from the active layer. After the charge separation process, the charge carriers have to be transported to these electrodes without recombination in the active layer. Finally, it is important that the charges can enter the external circuit at the electrodes without interface problems [3]. In general, for a successful organic photovoltaic cell, the operation can be summarized in five fundamental steps [2, 3]:

1. Absorption of photons in the polymer active layer that leads to the generation of excitons
2. Diffusion of excitons to an active interface

3. Charge separation into free electrons and holes
4. Charge transport
5. Charge collection

2.1.2.1 Light absorption

To achieve an efficient collection of the incident photons, the absorption spectrum of the active layer of the OPV should ideally match the solar emission spectrum. Another requirement, to achieve an efficient collection of photons is the active layer should be sufficiently thick to absorb most of the incident light [3].

The absorption coefficient spectra of organic active layers such as P3HT lack absorption in the red and near infrared part (NIR) of the spectrum (See Fig. 2.2-b) [3]. This means that these materials are not absorbing over the entire solar emission spectrum, just a portion of it, which in this case is in the waveband 300-700nm [7]. For a photovoltaic cell based on a single active layer material, it is found that a band gap of approximately 1.1 eV is optimal. By lowering the band gap of the organic material, it is possible to harvest more sunlight and therefore an increase in the photocurrent can be expected. For this increase in yield, much research effort is presently devoted to obtain organic polymers with an optical absorption band in the near infra-red (NIR), these are referred to as low band gap polymers [3].

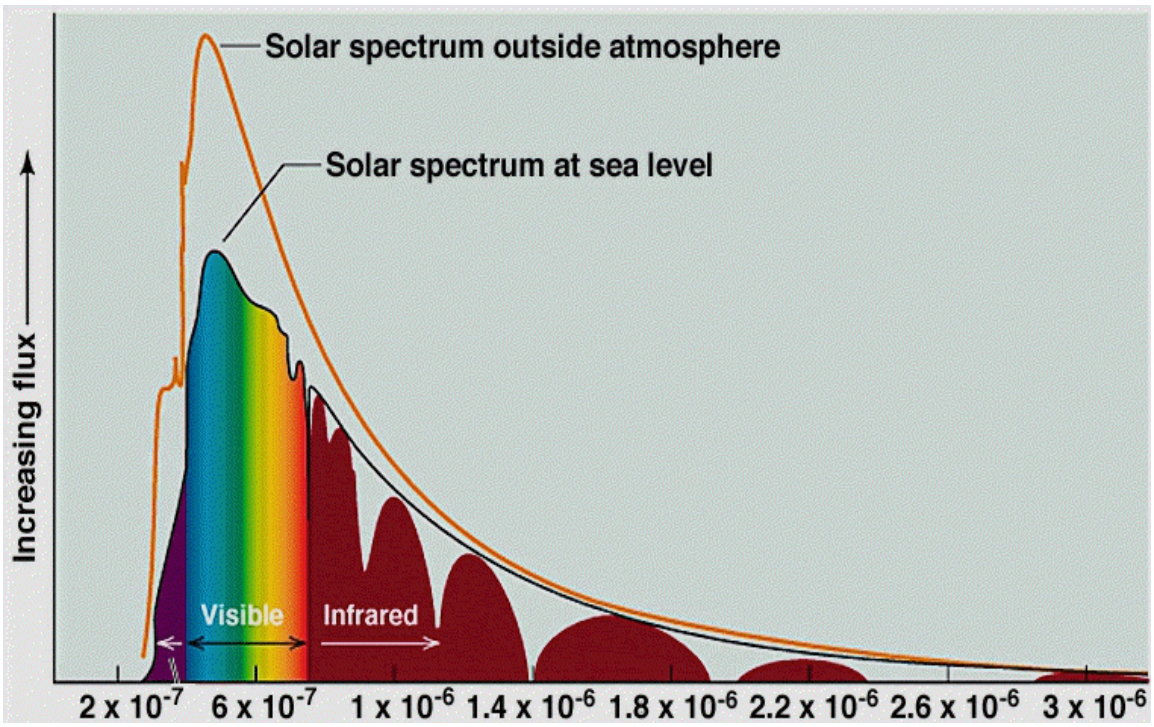

(a)

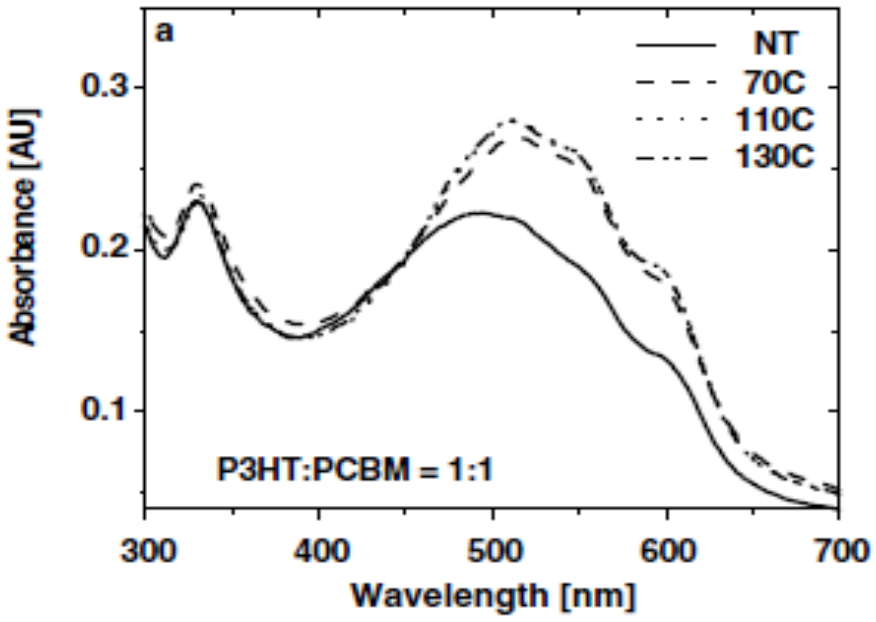

(b)

Figure 2.2. (a) The solar emission spectrum of the Sun between sea level and outside of the atmosphere [5]. (b) The absorption spectrum of P3HT:PCBM organic blend [6] as a function of post-deposition annealing temperature.

2.1.2.2 Exciton transport

To obtain an efficient organic solar cell, all excitons formed due to light absorption should lead to the formation of free charge carriers. Unfortunately, all excitons that are formed do not lead to free charge carriers; exciton transport is in competition with decay processes such as luminescence, geminate recombination, Langevin and radiative recombination to the ground state. The lifetime of an exciton is determined from the sum of the reciprocal value of all radiative and non-radiative decay times together. In an efficient solar cell, all excitons have to reach the photo-active interface within the exciton lifetime, τ_{exc}. The exciton transport occurs by diffusion and the distance an exciton is able to cross, L_{exc}, is given by [3]:

$$L_{exc} = \sqrt{D_{exc}\,\tau_{exc}} \qquad (2.1)$$

Where, D_{exc} is the diffusion coefficient of the excitons. For molecular materials, τ_{exc} is often several nanoseconds at most and therefore the distance, L_{exc}, is generally limited to ~10nm. In practice this implies that only those excitons formed within a distance of L_{exc} from the photoactive interface will contribute to charge separation. To minimize this problem, research has been devoted to increasing the diffusion coefficient of the excitons or to make the interfacial area much larger, so that each generated exciton is always close to an interface [3].

2.1.2.3 Charge separation

In the majority of organic solar cells, charges are created by photo-induced electron transfer. In this process, an electron is transferred from a donor material to an acceptor material with the aid of the additional input energy of an absorbed photon. An electron donor is characterized by a molecular material with a small electron affinity. On

the other hand an electron acceptor is a material with a high electron affinity. The difference between these electron affinity levels is the driving force required for the exciton dissociation [3].

It is essential that the charge-separated state is the thermodynamically and kinetically most favorable pathway for the exciton in order to achieve efficient charge generation. Thus, it is important that the energy of the absorbed photon is used for generation of the charge-separated state and is not lost via competitive processes like fluorescence, geminate recombination, or non-radiative decay. In addition to the conditions mentioned, the charge-separated state should be stabilized, to ensure the photo-generated charges can migrate to the respective electrodes. Therefore, recombination should be slowed down as much as possible [3].

2.1.2.4 Charge transport

In organic solar cells, after the charge transfer, the electrons and holes are in close proximity. Therefore there is a large chemical potential gradient that drives the charge carriers away from the exciton dissociating interface [3].

It is not yet clear to what extent the internal electrical field contributes to the charge transport in organic solar cells. This is due to the differences in mobilities in molecular materials compared to inorganic semiconductors [3].

2.1.2.5 Charge collection

The collection of charge carriers at the electrodes is often accomplished by utilizing a transparent conductive oxide (TCO), such as ITO as one electrode (anode) and a metal electrode, such as Aluminum on the other side of the active layer (cathode). Care has to be taken so that an ohmic contact between the electrodes and the molecular layers

is formed. In practice, special contact layers have been developed to obtain better performance of the solar cell. Examples of contact layers are a PEDOT:PSS layer, which is a charged conducting polymer layer at the TCO side. The exact reason how these layers improve the cells is unclear [3].

For an OPV based on two photo-active materials, optical excitation leads to the formation of excitons in one of the layers. For the charge separation process part of the original energy of the photon is lost, yielding an electron in the n-type material and a possible charge carrier in the p-type material [3].

2.2 Materials

The materials chosen to fabricate a polymer solar cell are crucial to achieve the desired power conversion efficiency (PCE). In this following subsection, OPV materials will be sorted into different groups based on functions (donor and acceptor) [8].

2.2.1 Donor Material

Polythiophene and its derivatives, such as Poly(3-alkylthiophene)s (P3AT) have been used as active material for optoelectronic devices, especially for photovoltaic cells. As mentioned above, P3HT is the best one in P3ATs as photovoltaic material and has become the most studied donor material for OPV technology [8].

2, 1, 3-Benzothiadiazole (BT) has been widely used as electron deficient building block in conjugated polymers with donor/acceptor structures. This category of polymer donors has been comprehensively studied and showed outstanding photovoltaic performances (summarized in [8]).

Pyrrolo[3,4-c]pyrrole-1,4-dione (DPP) Derivatives. DPP and its derivatives, usually have strong absorption bands in the visible range. Thiophene-based DPP

derivatives have well-confined conjugated structures, and exhibit good charge-carrier mobilities for both holes and electrons [8].

Benzo[1,2-b;4,5-b0]dithiophene-Based Polymers. There are three kinds of functional groups, including alkoxy, alkyl, and alkylthiophene, that were used as side groups on the 4- and 8-positions of the BDT unit to make solution-processable polymers [8].

2.2.2 Acceptor Material

Fullerene C_{60} has well-symmetric structure and exhibits good electron mobility. In order to improve its solubility and also to avoid severe phase separation of donor/acceptor blend, [6,6]-phenyl-C_{61}-butyric acid methyl ester ($PC_{60}BM$) was applied in OPVs. In the past decade, $PC_{60}BM$ and its corresponding C_{70} derivative ($PC_{70}BM$) have been dominantly used as acceptors in OPVs [8].

Indene-C_{60} Bisadduct and Indene-C_{70} Bisadduct (ICBA). Indene-fullerene adducts were used as electron acceptor materials in OPVs [8]. In addition, there are some other fullerene derivatives for application as acceptors in PSCs reported in literature, such as $PC_{84}BM$ and endohedral fullerenes and so on [8].

2.2.3 The Gold Standard

Despite their low efficiency, the organic polymers have attracted much interest. The poly(3-hexylthiophene) (P3HT) and [6,6]-phenyl C_{61}-butyric acid methyl ester (PCBM) blend is one of the promising organic solar cell materials. It is the most studied OPV to date and therefore has become the golden standard of OPV technology [4, 8].

There are a variety of other organic polymer materials, as stated above, however, the bulk of research remains by comparison to P3HT:PCBM. Thus far, there have also

been no radiation data on other materials of the cells. There is a lot of literature on these different materials and P3HT:PCBM because of the potential for high PCE, but no radiation data has been analyzed for any of these combinations of organic materials. There is little research of irradiation for P3HT:PCBM, especially for space based applications [9].

The polymer P3HT has been chosen as the golden standard because 10 years ago, it had the highest PCE to date at 4% [4]. The absorption spectrum of this material is shown in Fig. 2.2b. The absorption peak coincides with the peak of the solar spectrum peak; however, it far from absorbs over the full solar spectrum. This is why research is being carried out on other materials to achieve the absorption spectrum that differs from P3HT to eventually be able to yield tandem devices.

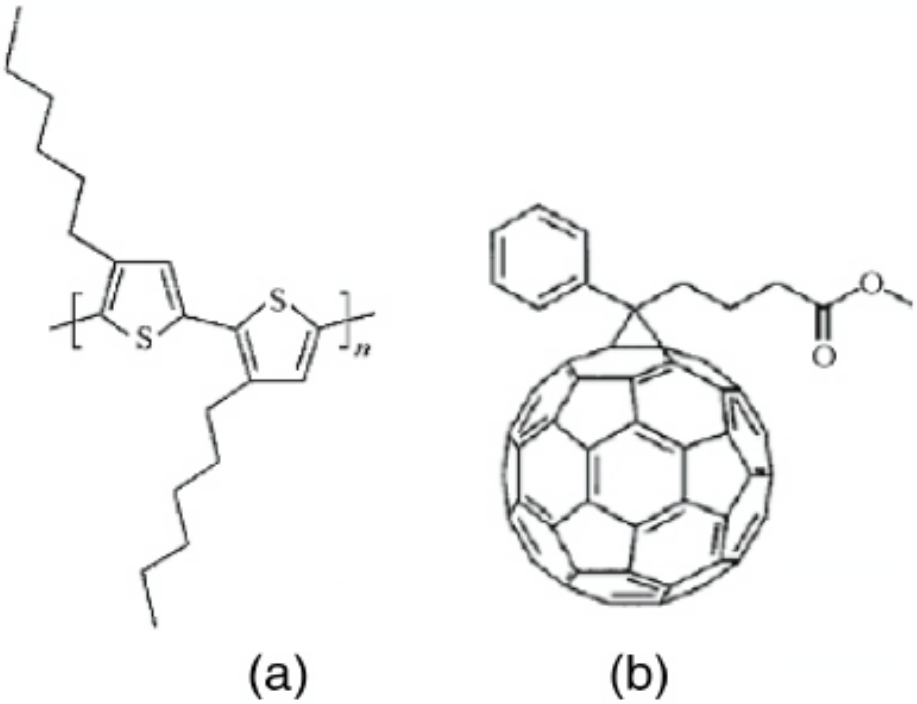

Figure 2.3. (a) Molecular diagram of P3HT. (b) Molecular diagram of PCBM [19].

2.3 What has been done

As mentioned previously, organic devices based on polymer:fullerene blend thin films are attracting extensive interest as low cost solar cells, with power conversion efficiencies approaching 12% [11]. It is argued by a variety of researchers that improvements in performance are dependent on developing a better understanding of the fundamental physics, as well as the pertinent loss processes in the blend. A better understanding of the loss processes such as bimolecular recombination, monomolecular recombination, geminate recombination, shunts, and leakage is required in order to increase device performance [8, 12]. In order to obtain a reliable hypothesis and model, researchers have developed measurement techniques and extraction methods to determine charge carrier densities, and carrier lifetimes in real devices under standard operating conditions, as well as open circuit voltage, short circuit current densities, capacitance, etc. [8].

2.3.1 Measurements

To obtain the measurements mentioned above, researchers have used a variety of experimental procedures. Beginning with the open circuit voltage parameter, researchers such as Shuttle, et al. [8] used multimeters for measurement. The short circuit current was measured using transient photovoltage (TPV) measurements and inserting a resistive load ~50 Ω on the diode output [8]. Full details of the extraction methods are found in [8, 12, 13].

The extraction of the open circuit voltage and the short circuit current densities was performed in order to obtain a J_{sc} vs V_{oc} comparison. Shuttle et al. [12] examined the

J_{sc} dependence on the charge carrier density. Thakur et al. [14] examined the temperature dependence of J_{sc} in order to determine the role of leakage current.

The relaxation time was measured using a variety of different techniques. Shuttle et al. used TPV measurements complemented with the use of transient absorption spectroscopy (TAS) measurements for comparison [8]. The details of the TPV measurements are outlined in section 3 and can also be found in [8, 12]. The other relaxation time extraction methods include Photo-CELIV, double injection currents, and integral mode time of flight [8, 15, 16].

The charge carrier densities are one of the most important terms in understanding the fundamental physics. The technique of charge extraction (CE) was developed by Shuttle et al. [8]. All other research groups utilize Shuttle's charge extraction techniques in order to obtain their charge carrier densities [8, 12, 13, 17, 16]. Belemonte [20], uses impedance spectroscopy measurements to determine the capacitance of the OPV. The low frequency arc is attributed to recombination in the photoactive blend and the capacitance, resistance, and lifetime values are a function of the bias voltage [20].

2.3.2 Data Analysis and interpretation

In the design of organic semiconductor materials and devices, we want to be able to predict the current density-voltage (J-V) behavior of a device from details of the device structure and material parameters [12]. Determining the origin of the J-V behavior is clearly a prerequisite for improving material and device design, but requires determination of J(n), R(n) and $n(V_{oc})$, where n is the total photo-induced carrier density [12].

Typical device variability of P3HT:PCBM V_{oc} ranges from 0 – 0.55V. Based on the TPV measurement utilized by Shuttle [8, 12], Gluecker [17], Foertig, et al. [13] typical carrier relaxation times range from 10 us – 3000 us. Fig. 2.4 is a comparative plot of relaxation time versus open circuit voltage obtained by extracting data from various publications [8, 13] and shown below.

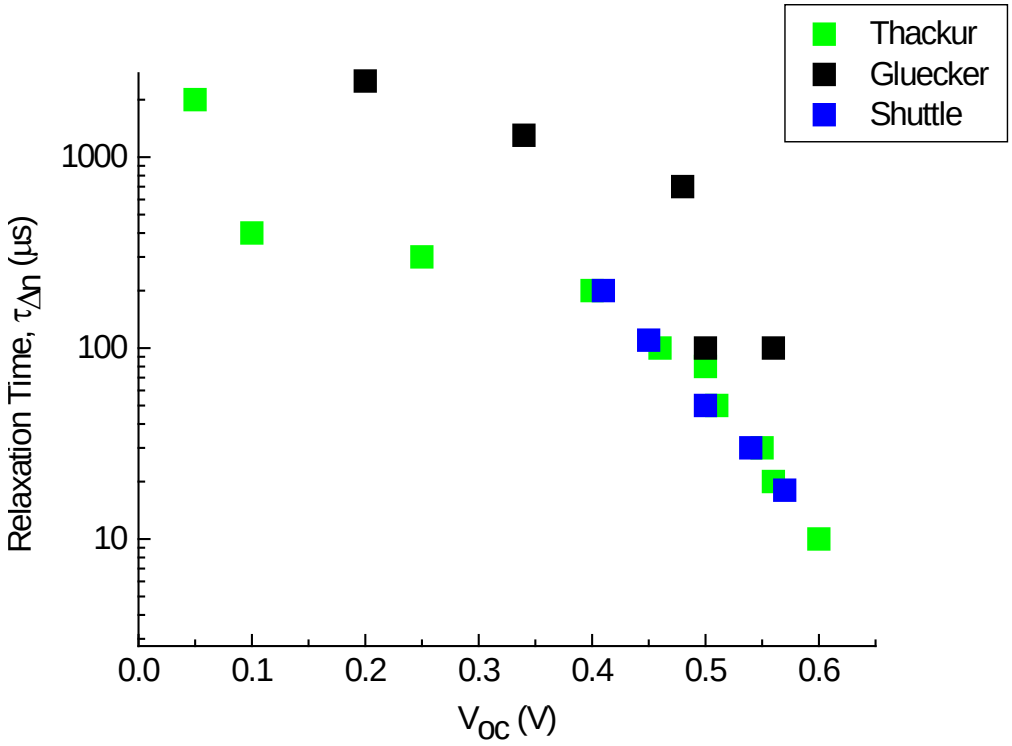

Figure 2.4. Relaxation time as a function of open circuit voltage from a variety of publications [8, 13, 16].

An alternative method was used by Thakur et al. [16] with a different technique to extract the relaxation time, however, the results of this paper are comparable for 0.3 V ≤ V_{oc} ≤ 0.6 V but significantly different than the results obtained by previous mentioned authors [8, 13] out of that range. The data is also shown in Fig. 2.4.

The dominant charge carrier extraction method, developed by Shuttle et al. [8], is utilized by a variety of other authors (for example [8-16]). Many others use this charge

extraction method to obtain charge, capacitance, and charge carrier density. In the published data that I have found, they do not obtain data at such a high open circuit potential, as in this study.. Typical charge carrier densities are plotted as a function of V_{oc} in Fig. 2.5 as a comparison between published authors [8. 17].

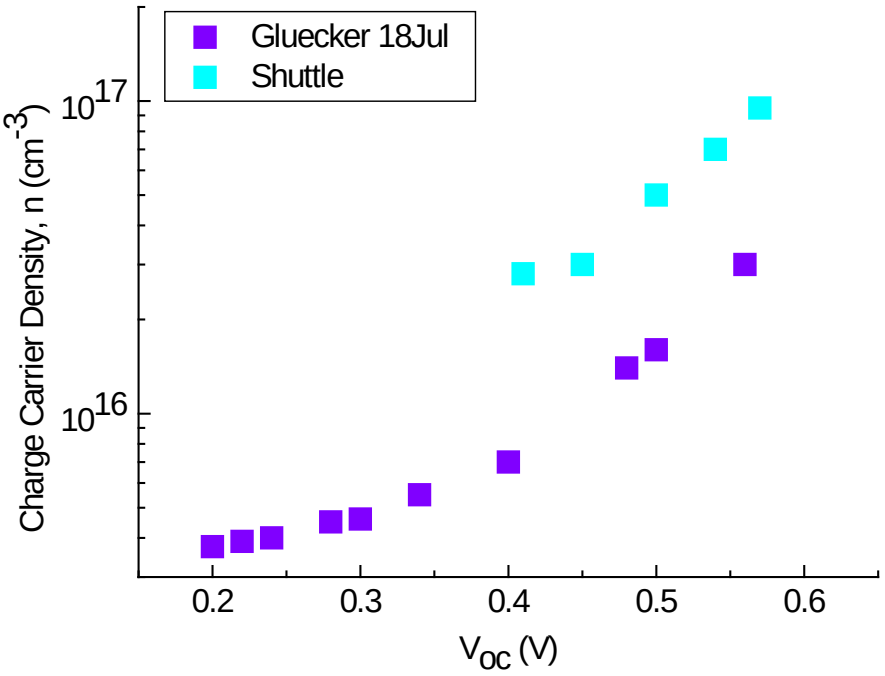

Figure 2.52. Charge carrier density as a function of open circuit voltage from different authors [8, 17].

The loss mechanism is argued to be via the Langevin interaction [8, 13]. Shuttle et al. [8] claim it varies proportional to n^3. A variety of other research groups have also found this effect, such as Foertig [13], Deibel [15], Juska, et al. [18]. Foertig et al. [12] have extracted the Langevin coefficient by initially plotting relaxation time (τ) as a function of the inverse charge carrier density (n). By differentiating this curve, one then find the slope, which is the Langevin coefficient (γ). Plotted in Fig. 2.6 is the extracted Langevin coefficient versus charge carrier density from the authors Foertig et al. [13]. I

have also extracted data from Shuttle et al. [8] to compare with Foertig et al. [13] as shown below.

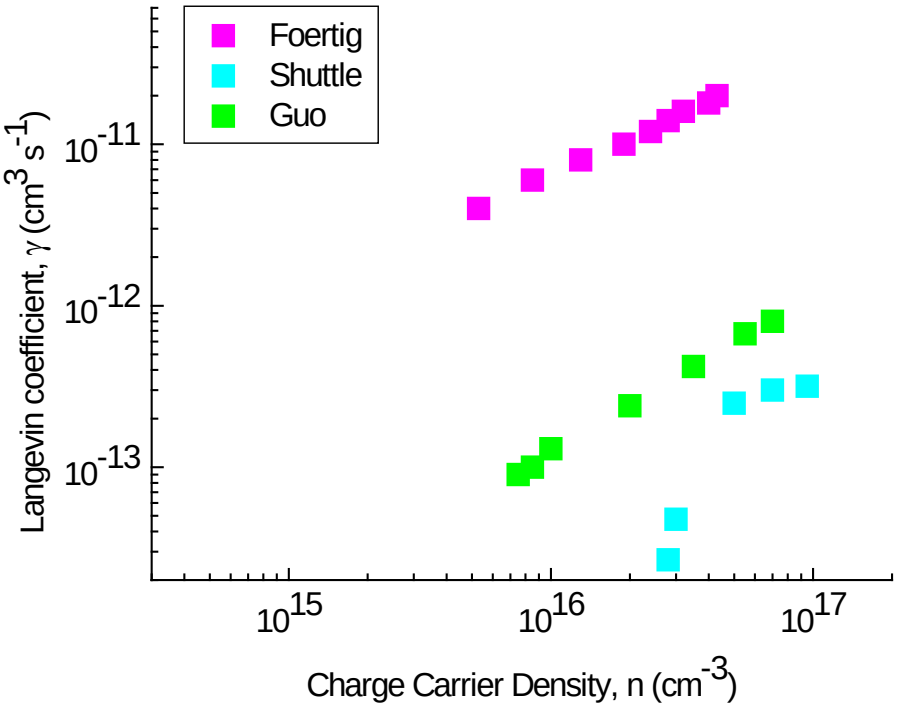

Figure 2.6. Figure about the Langevin coefficient as a function of charge carrier density for different authors [7, 8, 13].

Observe that there is a log relationship at the higher charge carrier concentrations between Foertig [13], Guo [7], and Shuttle [8] et al.

2.3.3 Conclusions

The agreement between researchers is that the Langevin coefficient varies with n and thus giving a n^3 dependence as shown in Fig. 2.6, which is inconsistent with the Langevin theory. The coefficient, γ, should not vary with n if Langevin recombination is the dominant mechanism.

The data of relaxation time versus V_{oc} match each other within experimental error as shown in Fig. 2.4 at least for V_{oc} > 0.3 V. Below 0.3 V, most authors do not report measured data.

The progress on the research on organic photovoltaics has increased our fundamental understanding of the physics and chemistry of the materials involved, however, it is far from complete. The application of these OPVs in general goes beyond our complete fundamental understanding of how they function. A model needs to be created that explains the fundamental physics within the whole range of the relaxation times, not just for V_{oc} >0.3V. Furthermore, there is no in-depth radiation effect data available from other authors on organic photovoltaics leaving a variety of physics left to explore and explain. All data to date by these researchers pertains to terrestrial applications and understanding. As a potential for space based applications, other measurements and analysis are needed, this is the subject of chapter 4.

2.4 References for Chapter 2

[1] Li, G., Shrotriya, V., Huang, J., Yao, Y., Moriarty, T., Emery, K., & Yang, Y. (2005). High-efficiency solution processable polymer photovoltaic cells by self-organization of polymer blends. *Nature materials*, *4*(11), 864-868.

[2] Kumar, A., Sista, S., & Yang, Y. (2009). Dipole induced anomalous S-shape< equation> IV</equation> curves in polymer solar cells. *Journal of Applied Physics*, *105*(9), 094512-094512.

[3] T. Savenije, *ORGANIC SOLAR CELLS*. Delft University of Technology.

[4] Weihao, G. (2009). An overview on P3HT: PCBM, the most efficient organic solar cell material so far. *Solid State Physics II,-, p. Online*.

[5] Unknown. (2013, January 5). Retrieved February 24, 2014 from http://physics.stackexchange.com/questions/48399/is-there-something-special-in-the-visible-part-of-electromagnetic-spectrum

[6] Li, G., Shrotriya, V., Yao, Y., & Yang, Y. (2005). Investigation of annealing effects and film thickness dependence of polymer solar cells based on poly (3-hexylthiophene). *Journal of Applied Physics, 98*(4), 043704.

[7] Hou, J., & Guo, X. (2013). Active Layer Materials for Organic Solar Cells. In *Organic Solar Cells* (pp. 17-42). Springer London.

[8] Shuttle, C. G., O'Regan, B., Ballantyne, A. M., Nelson, J., Bradley, D. D. C., De Mello, J., & Durrant, J. R. (2008). Experimental determination of the rate law for charge carrier decay in a polythiophene: Fullerene solar cell. *Applied Physics Letters*, *92*(9), 3311.

[9] C. Kouhestani, K. Kambour, D. Nguyen, C. Mayberry, R. A. B. Devine, C-C. Chen, G. Li and Y. Yang, "Mechanism of Carrier Relaxation in Unirradiated P3HT:PCBM Organic Photo-Cells I. Experiment," (to be published) 2014.

[10] Li, G., Shrotriya, V., Huang, J., Yao, Y., Moriarty, T., Emery, K., & Yang, Y. (2005). High-efficiency solution processable polymer photovoltaic cells by self-organization of polymer blends. *Nature materials*, *4*(11), 864-868.

[11] Kambour, K., Rosen, N., Kouhestani, C., Nguyen, D., Mayberry, C., Devine, R. A., ... & Yang, Y. (2012). Modeling of the X-irradiation Response of the Carrier Relaxation Time in P3HT: PCBM Organic-Based Photocells. *Nuclear Science, IEEE Transactions on*, *59*(6), 2902-2908.

[12] Shuttle, C. G., Hamilton, R., O'Regan, B. C., Nelson, J. A., & Durrant, J. R. (2010). Charge-density-based analysis of the current–voltage response of polythiophene/fullerene photovoltaic devices. *Proceedings of the National Academy of Sciences*, *107*(38), 16448-16452.

[13] Foertig, A., Baumann, A., Rauh, D., Dyakonov, V., & Deibel, C. (2009). Charge carrier concentration and temperature dependent recombination in polymer-fullerene solar cells. *Applied Physics Letters*, *95*(5), 052104-052104.

[14] Thakur, A. K., Wantz, G., Garcia-Belmonte, G., Bisquert, J., & Hirsch, L. (2011). Temperature dependence of open-circuit voltage and recombination processes in polymer–fullerene based solar cells. *Solar Energy Materials and Solar Cells*, *95*(8), 2131-2135.

[15] Deibel, C., Baumann, A., & Dyakonov, V. (2008). Polaron recombination in pristine and annealed bulk heterojunction solar cells. *Applied Physics Letters*, *93*(16), 163303-163303.

[16] Thakur, A. K., Baboz, H., Wantz, G., Hodgkiss, J., & Hirsch, L. (2012). Relation between charge carrier density and lifetime in polymer-fullerene solar cells. *Journal of Applied Physics*, *112*(4), 044502.

[17] Gluecker, M., Foertig, A., Dyakonov, V., & Deibel, C. (2012). Impact of nongeminate recombination on the performance of pristine and annealed P3HT: PCBM solar cells. *physica status solidi (RRL)-Rapid Research Letters*, *6*(8), 337-339.

[18] Juska, G., Genevicius, K., Nekrasas, N., Sliauzys, G., & Dennler, G. (2008). Trimolecular recombination in polythiophene: fullerene bulk heterojunction solar cells. *Applied Physics Letters*, *93*(14), 143303-143303.

[19] Yang, S., Zhao, N., Zhang, L., Zhong, H., Liu, R., & Zou, B. (2012). Field-effect transistor-based solution-processed colloidal quantum dot photodetector with broad bandwidth into near-infrared region. *Nanotechnology*, *23*(25), 255203.

[20] Garcia-Belmonte, G., Boix, P. P., Bisquert, J., Sessolo, M., & Bolink, H. J. (2010). Simultaneous determination of carrier lifetime and electron density-of-states in P3HT: PCBM organic solar cells under illumination by impedance spectroscopy. *Solar Energy Materials and Solar Cells*, *94*(2), 366-375.

3 Chapter 3 – Experimental Methodology

A wide variety of experimental procedures has been implemented to gather the necessary data to accomplish the goals set out in the thesis statement. The measurements that are crucial to understanding the fundamental physics of these devices depend on the relaxation time of the photo-induced carriers, charge carrier density and I-V characteristics. For extraterrestrial applications, radiation effects on these parameters must also be analyzed. As mentioned previously, the solar cells themselves used in these experiments were produced at UCLA using methods described elsewhere [1]. The experiments were performed at the Air Force Research Labs for the Space Electronics Branch. The central and key equipment was the ARACOR 4100 Semiconductor Irradiation System which acted both as a dark environment probe station as well as a protected source of x-irradiation. Inside the ARACOR, there is a vacuum chuck that can be remotely controlled to maneuver the cell under test in three dimensions in order to place the device under the radiation source. We fabricated a test mount specifically to enable illumination of the device with a background light through the ITO layer whilst simultaneously permitting x-ray exposure if required (see Fig. 3.1a).

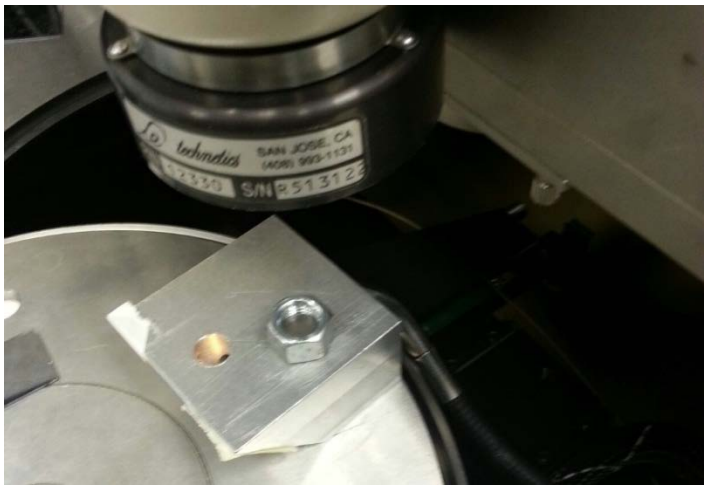

(a)

(b)

Figure 3.1. (a) An image of the block where the light is brought in via a fiber optic cable in the back and is reflected on a 45° angled mirror to bring the light under the device. (b) Overhead shot of the custom block showing the light being reflected off the mirror where the sample will be placed.

The Micro-Lite FL3000 is a halogen light source was used in the experiments to provide an un-calibrated background light level on the organic photovoltaic devices in order to vary the open circuit voltage, V_{oc}. This background light is brought into the

ARACOR via a fiber-optic cable to illuminate the device on the ITO side i.e. from the bottom side up (see Fig. 3.1a).

A General Radio 1531-AB Strobotac ,also a halogen light source, was used to superimpose a pulse of light on the background illumination (provided by the Micro-Lite FL3000) in order to generate a small increase in the generation of electron-hole pairs. The pulse of light is coupled into the background light by an aluminum block that is connected to the background light fiber-optic cable via a hole on the top that allows the pulse light to overlay. The resultant superimposed light is connected to the fiber-optic cable that illuminates the device. The pulse rate that is used in the experiments is ~2Hz and the illumination period is 2 μs per pulse (full pulse width at half pulse height)

A high input impedance Keithley 377 digital multi-meter (DMM) was used in these experiments to measure the open circuit voltage of the organic solar cell whilst the background light level was adjusted in intensity to generate the desired V_{oc}. An Agilent 54642 digitizing oscilloscope is used to measure the δV_{oc}(time) arising from the superimposed pulse signal that is illuminating the solar cell, in order to measure the relaxation time of the free electron-hole pairs. AC coupling was used in order to avoid a voltage offset due to the simultaneous presence of δV_{oc} and V_{oc} at the oscilloscope input. A typical waveform extracted in digital form from the oscilloscope is shown in Fig. 3.2

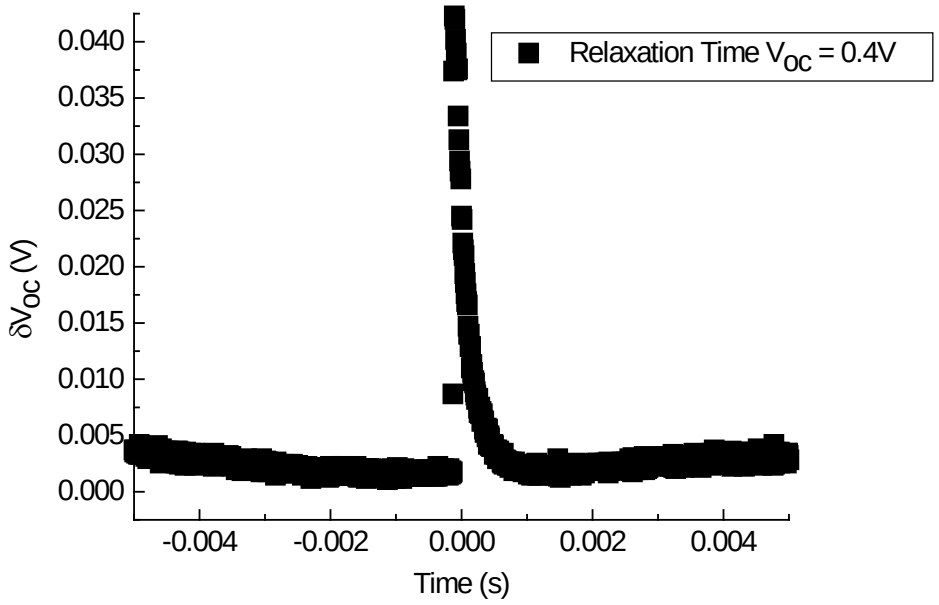

Figure 3.2. An image of the measured δV_{oc} on the oscilloscope.

For the charge carrier density measurements, a low value resistor is placed across the diode output and the voltage across it measured as a function of time. We will term this voltage δV_{sc}(time) and explain its relevance further below when we discuss how the charge carrier density is determined (described in detail in section 3.2.2.)

For DC measurements, in particular of the "static" current/voltage (I(V)) characteristic curves, an HP 4241B Modular DC Source is utilized. Variation of the applied DC voltage to characterize the device was enabled by a computer program called I-CV System Tools.

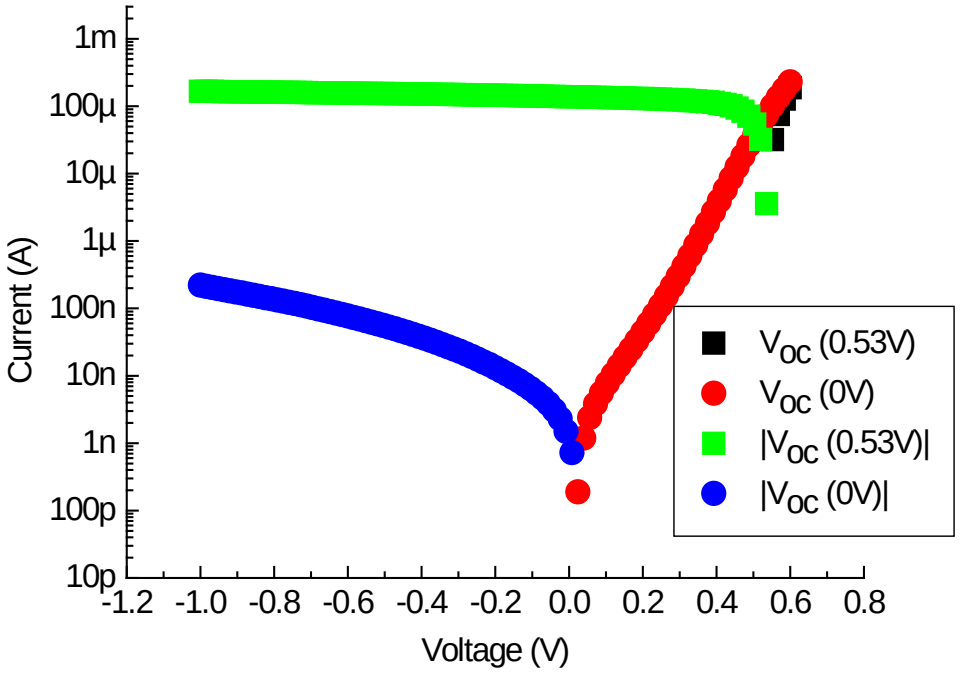

Figure 3.3. The I-V sweep at background light level of 0.53V is shown (■) as well as the magnitude (■) because these were negative, which does not show on a log plot. The I-V sweep for zero background light is also shown (●) as well as the magnitude (●) when the current drops below zero.

A typical I(V) dark current plot is shown in Fig. 3.3 together with the curve obtained with the background light set to induce a V_{oc} ~ 0.53 V.

3.1 Experimental Setup and Measurement Method

There are four categories of experiments that are utilized to extract the necessary parameters to begin to understand the fundamental physics of these devices. The relaxation time measurement, the charge carrier density measurement, the I-V curve measurement and radiation effect measurements are discussed.

3.1.1 Relaxation Time Extraction

The purpose of this experiment is to determine the relaxation time of the excess electron-hole pairs that are generated by superimposing light from the Strobotac on the

background light provided by the Micro-Lite FL3000. Our experimental set-up is analogous to the transient photovoltage measurements described by Shuttle et al. [3]. The key difference is that instead of a monochromatic laser, we use a stroboscope to generate the δV_{oc}.

The solar cell is placed upon the custom built block of aluminum such that the light from the Micro-Lite FL3000 will illuminate the device from the ITO side (see Fig. 3.1a). Probing of the cell anode and cathode contacts is achieved (Fig.3.4) using tungsten needles attached to adjustable probe arms. To ensure good electrical contact the anode and cathode finger contacts were covered with thin layers of indium.

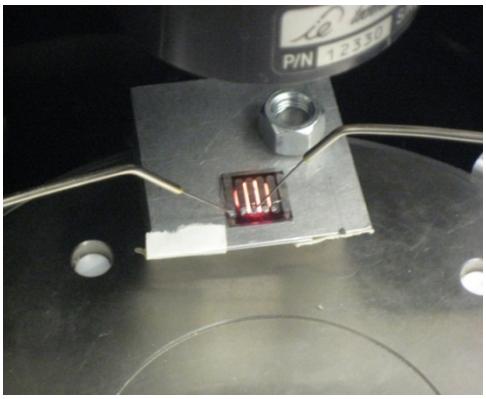

Figure 3.4. An image of a typical device on the custom built block.

From an experimental standpoint we were concerned from the outset with the potential significance of the magnitude of δV_{oc}. We therefore performed initial experiments in which we established a V_{oc} level; say 0.58 V, then adjusted the pulse intensity until δV_{oc} was ~ 50mV. We then adjusted V_{oc} and observed that δV_{oc} grew in amplitude as V_{oc} was decreased. In Fig. 3.5 we show the relaxation of δV_{oc} (□) with time for the case of a measurement at V_{oc} = 0.3V. We also show in the same figure δV_{oc} (time) data obtained when the peak or initial amplitude was decreased to 50 mV at each V_{oc} value (△). Note that for simplicity of comparison we have arbitrarily normalized the time

equal 0 values of δV_{oc} to unity in both cases (t = 0 being the peak of the exponential). Exponential relaxation fits to the two curves are indicated in blue for the "adjusted to 50 mV" case and green for the unadjusted case. In the former the relaxation time, τ, is 1.64 ms whereas in the latter not only is the fit quality degraded but the estimated relaxation time is 1.14 ms – significantly less than in the adjusted or what we will term the "small signal" case. We have not found reference to this effect in the published literature but to avoid substantial error we have taken the precaution in our measurements to remain in the small signal (δV_{oc}) limit.

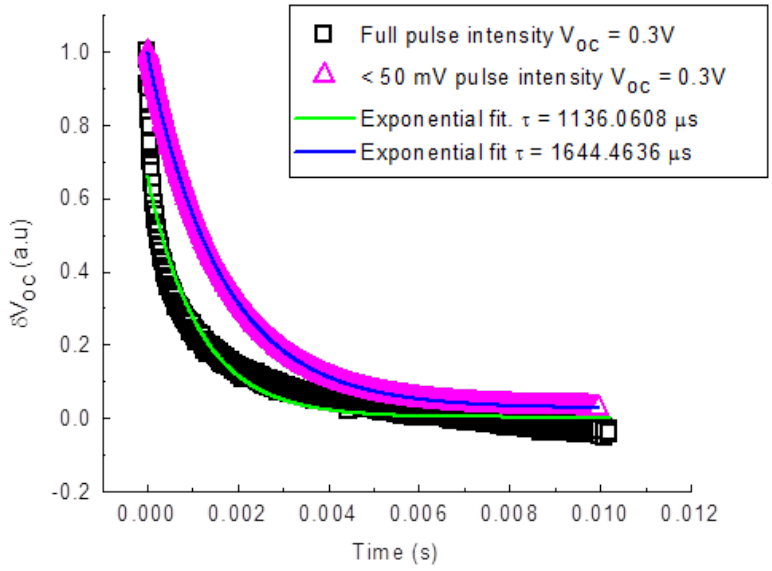

Figure 3.5. The δV_{oc} signal versus time as measured using the digital oscilloscope is shown as a comparison between adjusting the peak pulse intensity to ≤ 50mV (△) at any chosen V_{oc} and setting the initial δV_{oc} at 50 mV when V_{oc} = 0.55 V then not adjusting the pulse intensity (□) , both for V_{oc} = 0.3V. The green and blue fits correspond to the not adjusted and adjusted (≤ 50mV peak pulse intensity), respectively.

3.1.2 Charge Carrier Density Extraction

The purpose of this experiment is to extract the charge carrier density by measuring the exponential decay of the short circuit current δI_{sc} of the device. It was already shown [2] that a stroboscope, such as the Strobotac, is sufficient to perform

measurements of the relaxation time of the open-circuit voltage. Our experimental set-up is analogous to the transient photovoltage measurements [3]. The key difference between this measurement and the relaxation time extraction measurement is that we put a 470 Ω resistor across the photovoltaic cell output. We measure the photo-cell short circuit current (I_{sc}) by observing the voltage across the low value load resistor. Note that we observed the same δI_{sc} when using a 50 Ω load, but the measured voltage was, of course, smaller.

This experiment is performed under the same conditions as the relaxation time extraction experiment; however, instead of measuring the transient photovoltage, δV_{oc}, this measurement is extracting the transient photocurrent measured under approximately short circuit conditions by measuring δV_{sc} Note: the reason why 470Ω is considered short circuit is because 470Ω << 1MΩ input terminal on the oscilloscope.

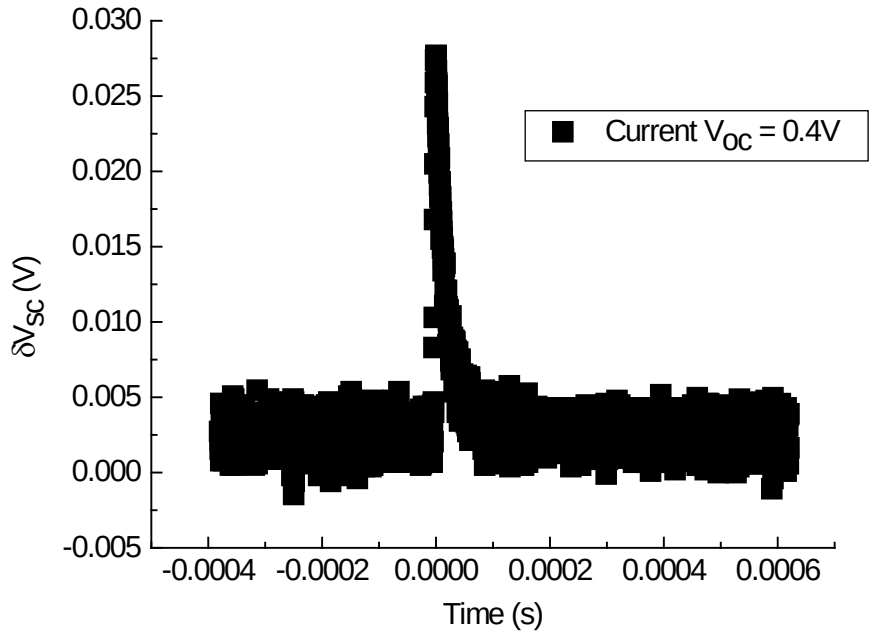

Figure 3.6. An image of the typical measured exponential decay under short circuit conditions on a device $\delta V_{sc}(t)$

3.1.3 Radiation Measurements

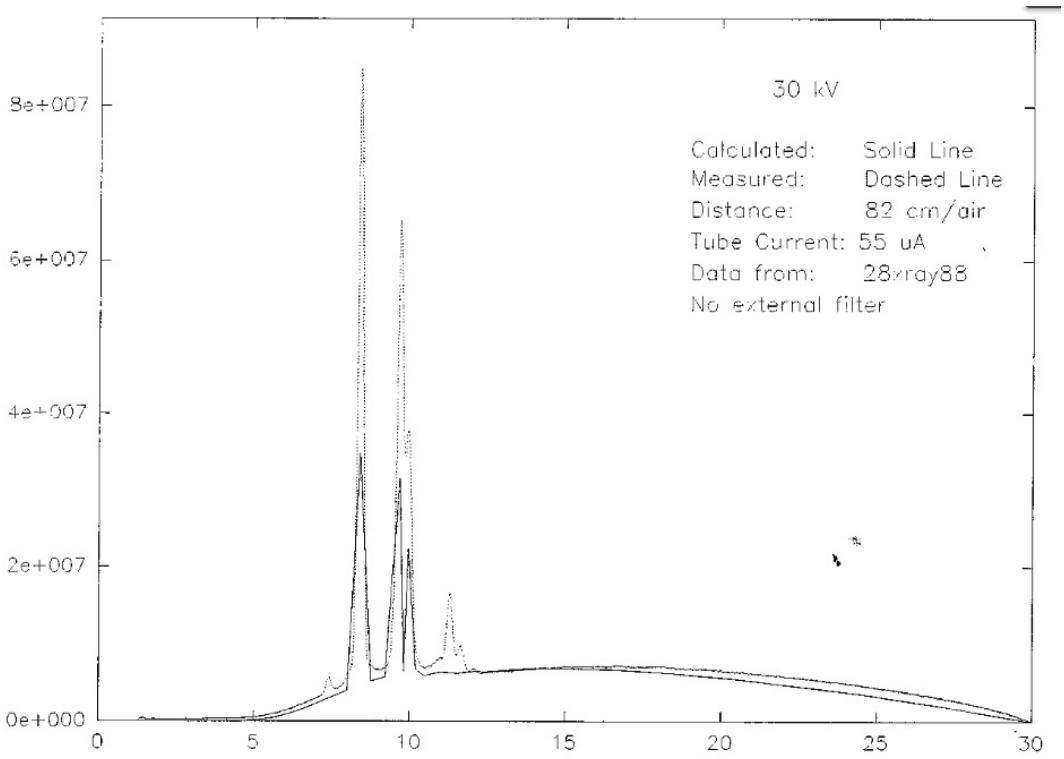

Figure 3.7. The x-irradiation spectrum of the tungsten target inside the ARACOR 4100 tube at 30 kV. The x-axis is in units of kV and the y axis is in units of particles exiting the tube.

The experimental set-up has been described elsewhere [5] and is briefly recalled as follows. Before any measurements are taken, the cooling system and safety electronics need to be activated. Once those systems are active, the x-ray tube needs to be "seasoned" to characterize the amount of radiation which is being provided and remove any remnant humidity in the high voltage area near the x-ray tube. As part of the seasoning process the output of the x-ray tube is first aligned with a calibrated silicon photo-diode so the tube output can be directly monitored. The x-ray tube is then subjected to different accelerating voltages and currents and the dose rate output directly measured in krads(Si)/minute. The maximum voltage/current couple is typically 60 kV/10 mA whilst the values chosen for the experiment are: the voltage is set to 45 kV

and the current to 20 mA to establish a radiation exposure dose rate of ~45 krads(Si)/min. For our experiments the more commonly used dose unit is rad(SiO_2). By dividing the rate in rads(Si) by 1.8 one obtains the radiation levels in rads(SiO_2), in our case, 25 krads(SiO_2)/ min. Since the devices that are being irradiated have a quartz cover slide which can attenuate the x-rays another parameter has to be factored into the characterization of the final amount of radiation exposure per minute. The attenuation factor for the quartz cover slide is 0.42. This was determined by placing a sample quartz cover slide provided by the manufacturer over the calibrated measurement diode. Upon the beginning of dosage, a calculator excel spread sheet was created to help with determine exposure times required to obtain desired overall doses. Measurements at the end of each exposure time were taken of the relaxation time, carrier density and I-V as described in sections 3.2.1, 3.2.2, and 3.2.3.

The equipment is set-up according to the flow diagram shown below.

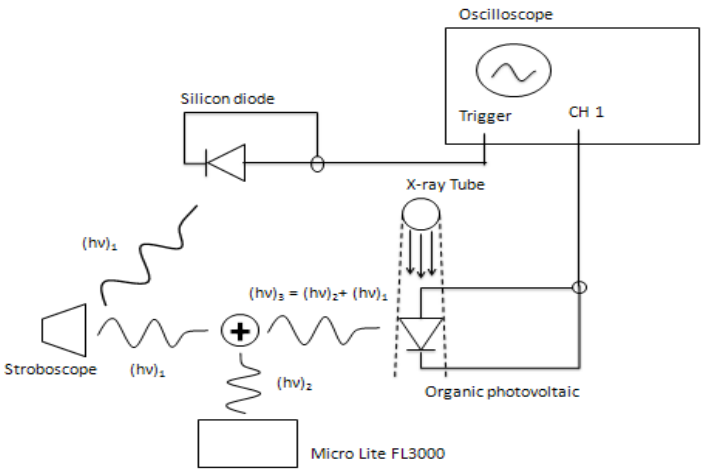

Figure 3.8. Schematic of the radiation testing set-up.

3.2 Data Breakdown

3.2.1 Relaxation Time Extraction

The extraction of the relaxation time from the data is a relatively simple procedure. Beginning with the highest V_{oc} established with the maximum continuous background light level we measure δV_{oc} (time) resulting from the imposed light pulse. Due to the initialization parameters of the oscilloscope and the triggering edge, the peak does not always align to the zero point in time. There is an adjustment that is made to make the time of the highest peak of δV_{oc} (time) on the measured data zero. A typical data set measured using the oscilloscope is shown in Fig. 3.9.

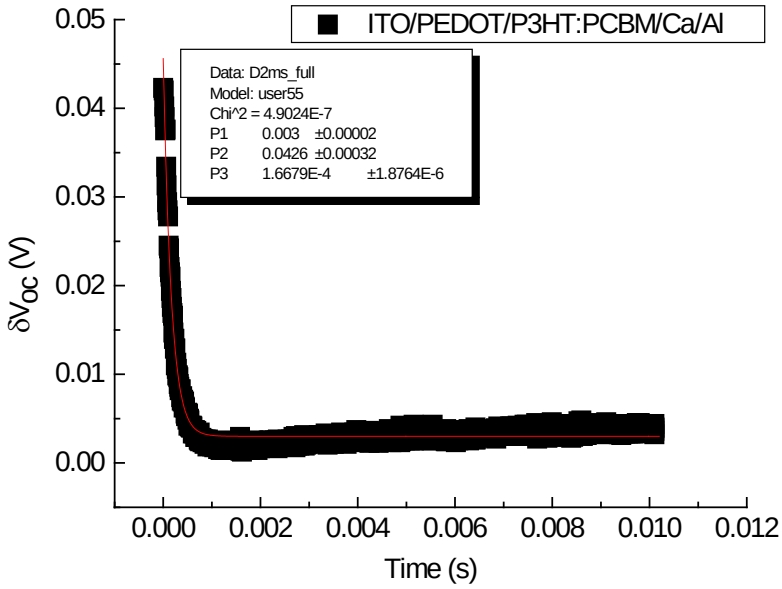

Figure 3.9. A plot from the background V_{oc} level of 0.4V of the time dependence of the pulse height (δV_{oc} (time)) shown by (■).

The red fitted line in Fig. 3.9 is obtained using Eq. 3.1 shown below. ORIGIN™ [6] plotting software has a non-linear curve fitting analysis facility built into the program, where one can create one's own fit equation to analyze the data that is plotted. The

equation used to fit this data in order to extract the relaxation time is derived elsewhere [5] but recalled here as:

$$\delta V_{oc} = A_r + B_r e^{-\frac{t}{\tau_{\Delta n}}} \quad (3.1)$$

where, A_r is an offset value in the y direction, B_r is the peak of the relaxation pulse, t is the time and $\tau_{\Delta n}$ is the relaxation time of the charge carriers. According to the fitting parameters in Origin 5.0, P1 is A_r, P2 is B_r, and P3 is $\tau_{\Delta n}$.

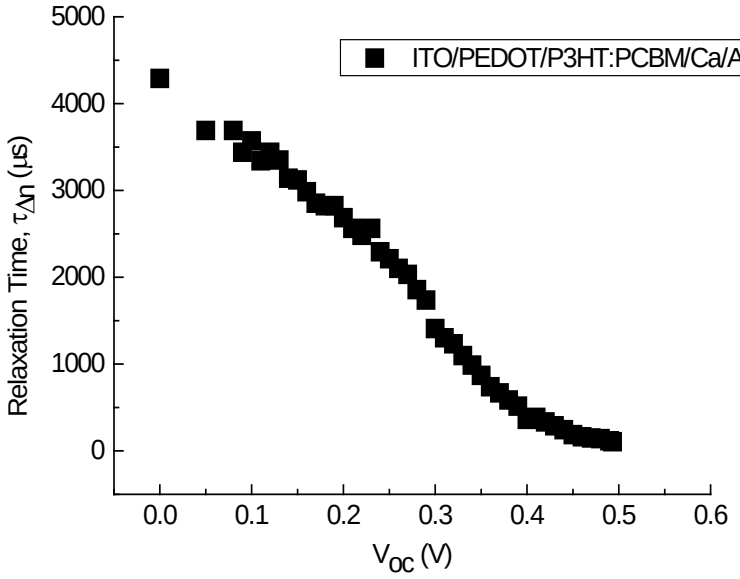

Figure 3.10. A typical plot of all the relaxation time values extracted as a function of V_{oc} measured on a device. δV_{oc} was adjusted by changing the light level of the pulse to ensure operation in the small perturbation regime.

ORIGIN 5.0 gives values for A_r, B_r and τ with error margins. The values are taken and put into an excel sheet template that was created to help make the process flow easier. It takes the equation fitted values and moves the values to make it easier to copy and paste those values into ORIGIN 5.0 to create the graphs that are required. Once the data that was taken has been plotted and fitted for each V_{oc} value measured, the next step is to plot all the fitted data for result analysis.

3.2.2 Charge Carrier Density Extraction

The breakdown method to extract the charge carrier density uses a similar approach to the relaxation time extraction; however, this extraction method requires more analysis. In this technique we measure the time dependent variation of the short circuit current voltage induced by the light pulse, δV_{sc} (time) A typical δV_{sc} (time) l data set measured by the oscilloscope is shown in Fig. 3.11.

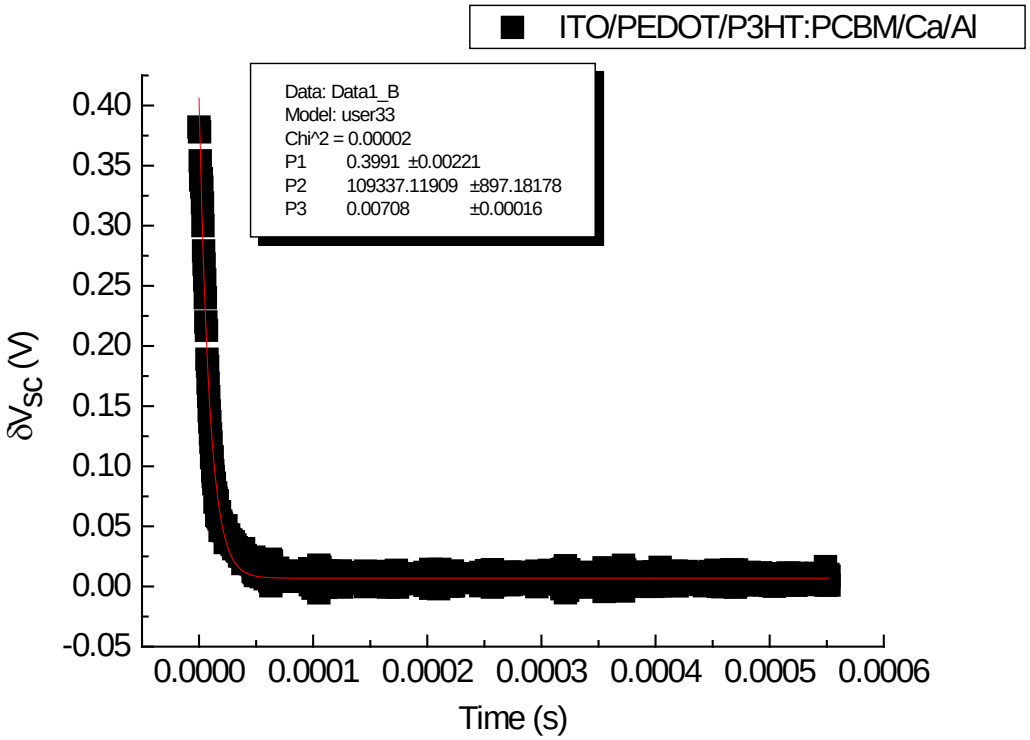

Figure 3.11. Plot of δV_{sc} (time) for V_{oc} = 0.40V from the peak of the pulse onward in time shown by (■). The red fitted line is obtained using Eq. 3.2 shown below. The data in the box are the fitting parameters that are used to extract the relaxation time.

Again using ORIGIN 5.0's non-linear curve fitting analysis function built into the program, plotted fit to the data is obtained. Dividing δV_{sc} by the short circuit load resistance (470 Ω) the time dependence of the short circuit current is obtained (δI_{sc} (time)

The equation used to fit this data in order to extract the relaxation time is one that is derived elsewhere [3] and is:

$$\delta V_{sc} = A_c * \mathbf{e}^{-\alpha t} + C_c \quad (3.2)$$

where A_c is the pre-factor, α is the inverse of τ, t is the time and C_c is offset of the current measurement. Note, we change the symbolism of Eq. 3.2 to Eq. 3.1 to remind the reader that one refers to δV_{oc} and the other relates to δV_{sc}. According to the fitting parameters in Origin 5.0, P1 is A_c, P2 is α, and P3 is C_c.

ORIGIN 5.0 provides values for A_c, α and C_c with error margins. Once the data that was taken has been plotted and fitted for each V_{oc} value measured, we use two different equations to get the charge and the capacitance for these V_{oc} values [3].

$$\boldsymbol{Q} = \left(\frac{\mathbf{Ac}}{\boldsymbol{\alpha} * \mathbf{R}}\right) \quad (3.3)$$

R is the short circuit load resistance used, in this case 470Ω [3]. The capacitance is then:

$$\mathbf{C} = \frac{\mathbf{Q}}{\mathbf{B_r}} \quad (3.4)$$

B_r is the peak of the voltage relaxation pulse (δV_{oc}).

The next step is to plot C versus V_{oc}, so I can perform a fit in the form of eq. 3.5 [3]:

$$\boldsymbol{C_{total} = Ae^{\alpha V_{oc}} + C_{geom} = C_{diff} + C_{geom}} \quad (3.5)$$

Where C_{total} is the total capacitance, A is a prefactor fit parameter, α is a fit parameter, V_{oc} is the open circuit voltage, C_{geom} is the geometrical capacitance, and C_{diff} is the differential capacitance. In order to derive the carrier density from this data, we must use the following equation [3]:

$$\boldsymbol{n = Z \int_0^{V_{oc}} C_{diff}\, dV} \quad (3.6)$$

Where n is the carrier density, Z is $\frac{1}{Area*e*thickness}$, V_{oc} is the open circuit voltage, C_{diff} is the differential capacitance. With this information we can now plot n versus V_{oc} or if we have already done the voltage relaxation time breakdown, τ versus n. A typical result set for $\tau(n)$ is shown in Fig. 3.12.

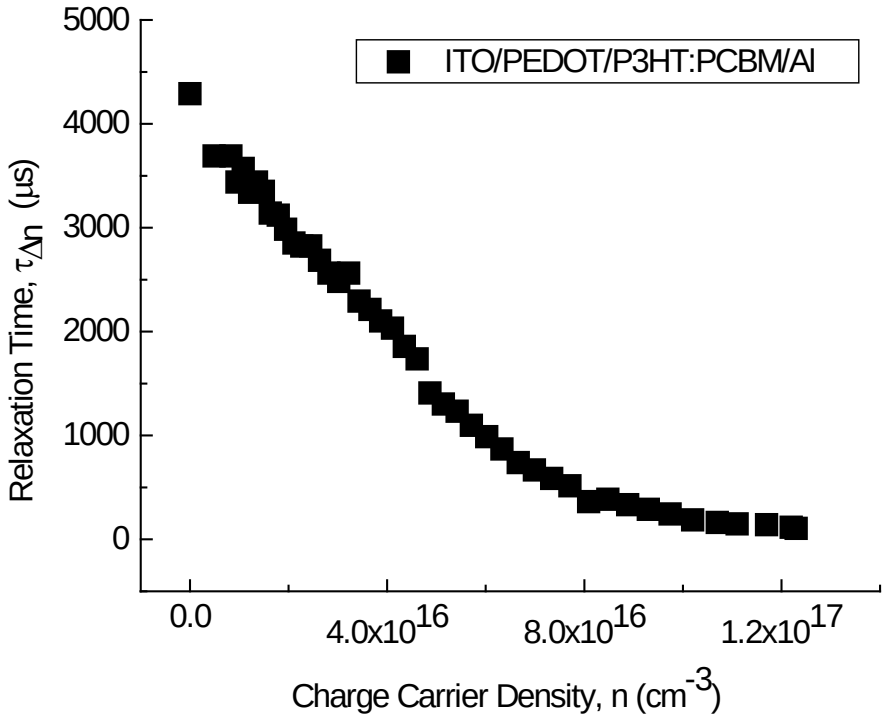

Figure 3.12. Plot of all the open circuit voltage relaxation times extracted for every carrier density values measured on this device (determined from short circuit current conditions).

3.3 References for Chapter 3

[1] Li, G., Shrotriya, V., Huang, J., Yao, Y., Moriarty, T., Emery, K., & Yang, Y. (2005). High-efficiency solution processable polymer photovoltaic cells by self-organization of polymer blends. *Nature materials*, *4*(11), 864-868.

[2] Mahan, J. E., Ekstedt, T. W., Frank, R. I., & Kaplow, R. (1979). Measurement of minority carrier lifetime in solar cells from photo-induced open-circuit voltage decay. *Electron Devices, IEEE Transactions on*, *26*(5), 733-739.

[3] Shuttle, C. G., ORegan, B., Ballantyne, A. M., Nelson, J., Bradley, D. D. C., De Mello, J., & Durrant, J. R. (2008). Experimental determination of the rate law for charge carrier decay in a polythiophene: Fullerene solar cell. *Applied Physics Letters*, *92*(9), 093311-093311.

[4] Kumar, A., Devine, R., Mayberry, C., Lei, B., Li, G., & Yang, Y. (2010). Origin of Radiation-Induced Degradation in Polymer Solar Cells. *Advanced Functional Materials*, *20*(16), 2729-2736.

[5] Kambour, K., Rosen, N., Kouhestani, C., Nguyen, D., Mayberry, C., Devine, R. A., ... & Yang, Y. (2012). Modeling of the X-irradiation Response of the Carrier Relaxation Time in P3HT: PCBM Organic-Based Photocells. *Nuclear Science, IEEE Transactions on*, *59*(6), 2902-2908.

[6] Origin 5.0. 1997. OriginLab Corporation., Northampton, MA, USA

4 Chapter 4 – Results and Discussion

In the previous chapters we discussed the advantages of OPV technology over classical inorganic semiconductor based cells. Our particular interests concern the applicability of organic photo-cells for use in space based solar panels where it must be recognized that "unusual" conditions exist which are not generally addressed by the organic photo-cell community [1]. In particular, we are concerned by radiation effects and very little work has been performed and reported in this area. The process flow by which OPV's are manufactured cannot yet be considered "stabilized" and therefore we anticipate that radiation response may well depend upon the origin of cells. In the following we will present and interpret the experimental data but before doing this we outline the underlying theory which will be necessary. In the first case we follow the modeling used by Shuttle et al. [2] in which we assume that the small open circuit voltage fluctuation with time ($\delta V_{oc}(t)$) induced by a light pulse can be written:

$$\frac{d\Delta V_{oc}}{dt} \propto \frac{d\Delta n}{dt} = -\frac{\Delta n}{\tau_{\Delta n}} \qquad (4.1)$$

where Δn is the change in carrier density at the top of the distribution induced by the background light level appropriate to a chosen V_{oc}. The relaxation time, $\tau_{\Delta n}$, associated with the small change in the carrier distribution density, Δn. Empirically one generates the equation [2]:

$$\boldsymbol{\tau_{\Delta n} = \tau_{\Delta n}^{0} e^{-\beta V_{oc}}} \qquad (7)$$

where $\beta = q/kT = 38.6\ eV^{-1}$ at room temperature. We therefore anticipate a plot of $\ln(\tau_{\Delta n})$ versus V_{oc} to be a straight line of slope $-\beta$. Such a relationship was indeed found by Shuttle et al. [2] over a limited range of V_{oc} (0.4 – 0.59 V) but with $\beta = 16\ eV^{-1}$. The origin of this discrepancy was not explained. As we go through the experimental data we

concentrate on an interpretation following Shuttle et al [2] and in particular interpretation of the data following the assumption of a Langevin like [2, 3] carrier relaxation model.

4.1 Un-irradiated Data

4.1.1 Relaxation Time vs V_{oc}

Using the methodology described in the previous chapter and adjusting the incident light pulse intensity to as best as possible work with small but constant δV_{oc}, we obtain the values of $\tau_{\Delta n}$ (V_{oc}) shown in Fig. 4.1. A notable reduction in the variation of $\tau_{\Delta n}$ with V_{oc} is observed for values of $V_{oc} \leq 0.3$ V. This regime has been little explored by other authors, presumably because it corresponds to very low light levels. In the linear region of $\ln(\tau_{\Delta n})$ versus V_{oc} we deduce $\beta = 19\ eV^{-1}$, larger than found by others [2] but still nearly a factor of two smaller than the expected value on the basis of a simple exponential law with $\beta = q/kT$. The current theory amongst other authors, mentioned in Chapter 2, is that Langevin is the dominant recombination mechanism [2, 3]. If that is the case, there should be no turn over at the lower light levels, unlike what is seen in Fig. 4.1. In fact, we have concluded from simulations [4],that this effect may in fact be attributed to the presence of an effective shunt resistance of the order of ~5MΩ in parallel with the ideal diode leading to an RC type time constant effect. This will be discussed further.

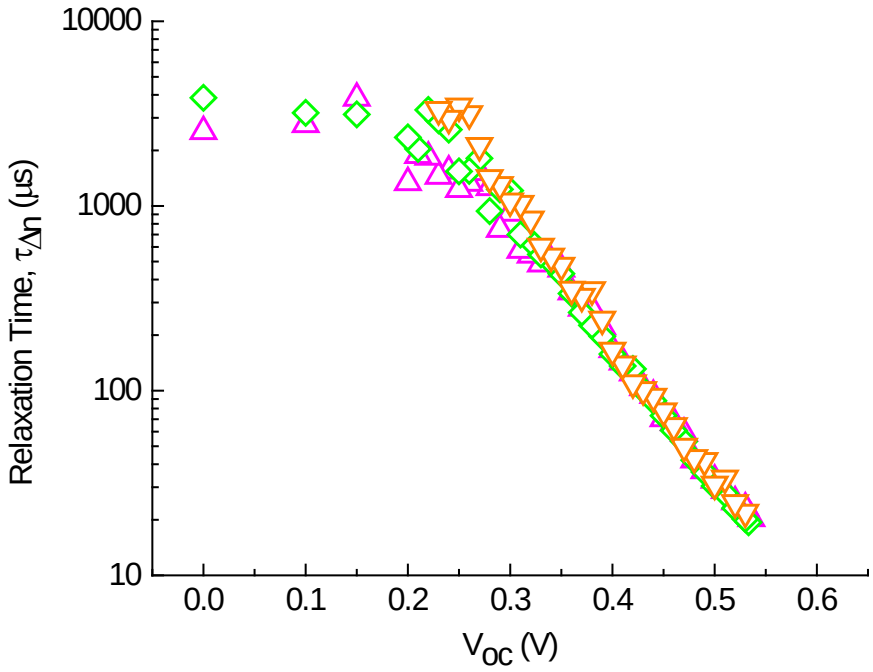

Figure 4.1. Photo-induced carrier relaxation time as a function of open circuit voltage for different devices from the same production batch. The δV_{oc} used to establish an out of equilibrium charge carrier population was adjusted to 50 mV for each V_{oc}. The (△) represents data from T66-F1, (◇) represents data from T66-F2, and (▽) represents data from T66-F3. Note: the nomenclature for these devices follows the sample number (T66) then the finger on that sample (-F1). In general up to five fingers per sample were usable.

At this point we must ask the question whether or not using the small pulse method we are measuring a relaxation time consistent with the total photo-carrier density (n) as generated by the background light level used to establish V_{oc}. Following the work of Shuttle et al. [2] appropriate to that case one can develop an expression for dn/dt of the form:

$$\frac{dn}{dt} = \frac{n^{1+\lambda}}{(1+\lambda)\tau_{\Delta n}^{0} n_0^{\lambda}} \qquad (8)$$

where $n = n_0 e^{\gamma' V_{oc}}$ and $\tau_{\Delta n} = \tau_{\Delta n}^{0} e^{-\beta V_{oc}}$ leading to $\frac{d\tau_{\Delta n}}{d\tau_{\Delta n}^{0}} = \left(\frac{n_0}{n}\right)^{\lambda}$. From these formulae $\lambda = \frac{\beta}{\gamma'}$. Writing $\frac{dn}{dt}$ in the form $\frac{dn}{dt} = -\frac{n}{\tau_n}$ we can easily demonstrate that $\tau_n = (1+\lambda)\,\tau_{\Delta n}^{0}$ so that in general the relaxation time of the total photo-induced carrier

population will be longer than the relaxation time deduced by transient photo-voltage methods. In order to pursue this further we need to determine $n(V_{oc})$ and hence, λ.

4.1.2 Charge Carrier Density vs V_{oc}

The total charge distribution density, $n(V_{oc})$, can be deduced by performing the integral defined in Chapter 3 and recalled here:

$$\boldsymbol{n(V_{oc}) = \frac{1}{Aqd}\int_0^{V_{oc}} C_{diff}\, dV} \qquad (9)$$

where n is the total charge carrier density, A is the device area, q is electronic charge, d is the thickness of the photoactive layer, and C_{diff} is the derived differential capacitance which will be evaluated later.

In Chapter 3 we explained the methodology for determining the charge Q by integration of the short circuit current pulse. Knowing the associated δV_{oc} associated with each Q value one can establish the differential capacitance (C_{diff}) curve (Fig. 4.2) from which one can determine the carrier density $n = n_0 e^{\gamma' V_{oc}}$ by integration (Fig. 4.3). However, before we do this we note that in Fig. 4.3, $\ln(C_{diff})$ is not a linear function of V_{oc} and for $V_{oc} \leq 0.3$ V there appears to be a tendency to a constant value of $C_{diff} \sim 3.7$ nF. The geometrical capacitance of the photo-cell can be calculated as:

$$\boldsymbol{C_{geom} = \frac{\varepsilon \varepsilon_0 A}{d}} \qquad (10)$$

where ε and ε_o have their usual meanings and A and d are the cell area and blend layer thickness; the value we calculate using this formula is 1.4 nF. This strongly suggests, as mentioned previously, that the $\tau_{\Delta n}$ behavior measured for $V_{oc} < 0.3$ V is in essence a reflection of an RC limiting time constant of the cell and is not related to relaxation of the photo-generated carriers.

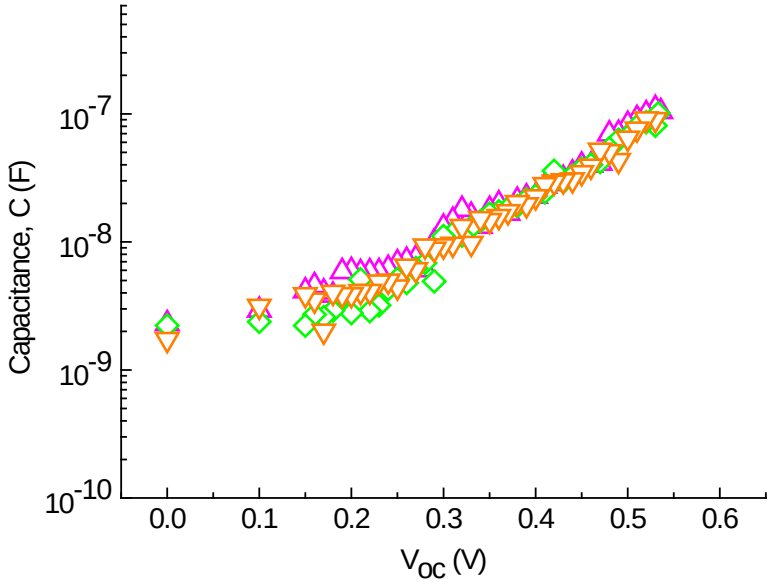

Figure 4.2. Differential capacitance as a function of open circuit voltage for different devices. The (△) represents data from T66-F1, (◇) represents data from T66-F2, and (▽) represents data from T66-F3. For an ideal diode $\ln(C_{diff})$ versus V_{oc} should be a straight line of slope q/2kT.

Correcting the data in Fig. 4.2 for the geometrical capacitance one can the perform the appropriate integrals to extract $n(V_{oc})$ – this data is shown in Fig. 4.3. From the slope of the plots one determines $\gamma' \sim 17V^{-1}$

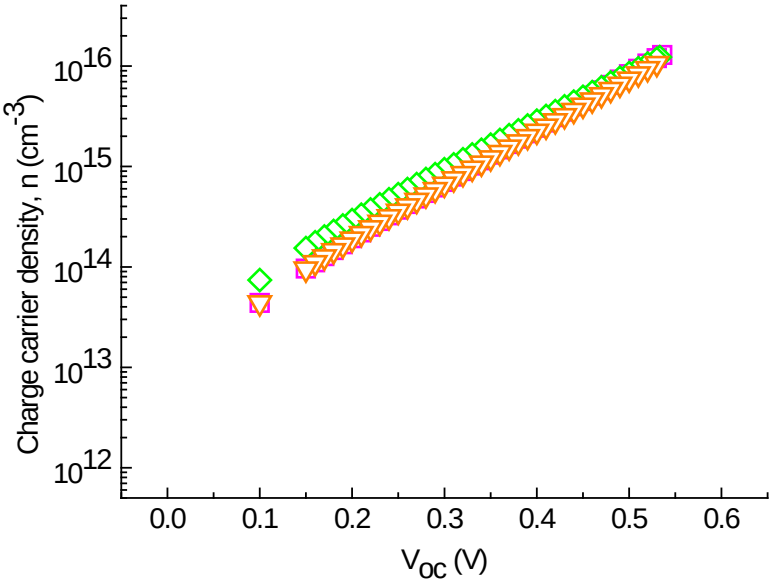

Figure 4.3. Charge carrier density as a function of open circuit voltage. The (△) represents data from T66-F1, (◇) represents data from T66-F2, and (▽) represents data from T66-F3.

We have underlined the fact that various authors consider the Langevin recombination mechanism to be the primary one in organic photo-voltaic cells. We therefore apply this model to examine its predictions concerning C_{diff}. With the Langevin recombination model one can determine V_{oc} [3]:

$$V_{oc} = \frac{E_{gap}}{q} - \frac{kT}{q}\ln\left(\frac{(1-P)\gamma N_c^2}{PG}\right) \tag{11}$$

Where E_{gap} is the effective bandgap, P is the dissociation probability of a bound electron-hole pair into free carriers, N_c is the effective density of states, γ is the Langevin recombination coefficient and G is the generation rate of bound electron-hole pairs. At equilibrium G may also be expressed as [3]:

$$G = \frac{\gamma np(1-P)}{P} \tag{12}$$

Where n (p) is the total photo-induced electron (hole) density which we write as n = p = Q/Ad. Then differentiating Eq. 5 with respect to V_{oc} we obtain $\frac{\frac{\delta G}{\delta V_{oc}}}{\sqrt{G}} \propto \frac{\delta Q}{\delta V_{oc}}$. Re-arrangement of Eq. 4.7 yields $G \propto e^{\frac{qV_{oc}}{kT}}$, which enables us to express the differential capacitance, C_{diff}, as:

$$C_{diff} = \frac{\delta Q}{\delta V_{oc}} \propto \frac{\frac{\delta G}{\delta V_{oc}}}{\sqrt{G}} \propto \frac{q}{2kT} e^{\frac{qV_{oc}}{2kT}} \quad (13)$$

Taking the derivative of $\ln(C_{diff})$ as a function of V_{oc} – we obtain values ~ 18 V^{-1}. If the Langevin approach is correct we should obtain a unique value of q/2kT equal to 19.3 eV^{-1}. This result appears to argue in favor of the Langevin model. From the published data of Shuttle et al. [2] we obtain a value of 6.3 $V^{-!}$.

4.1.3 Langevin Coefficient vs Charge Carrier Density

Having determined γ' and β we deduce λ = 1.4 from which we conclude that τ_n = 2.4 $\tau_{\Delta n}$. In Fig. 4.4a we plot $\tau_{\Delta n}$ as a function of the charge carrier density, n, and in Fig. 4.4b $\tau_{\Delta n}$ as a function of 1/n.

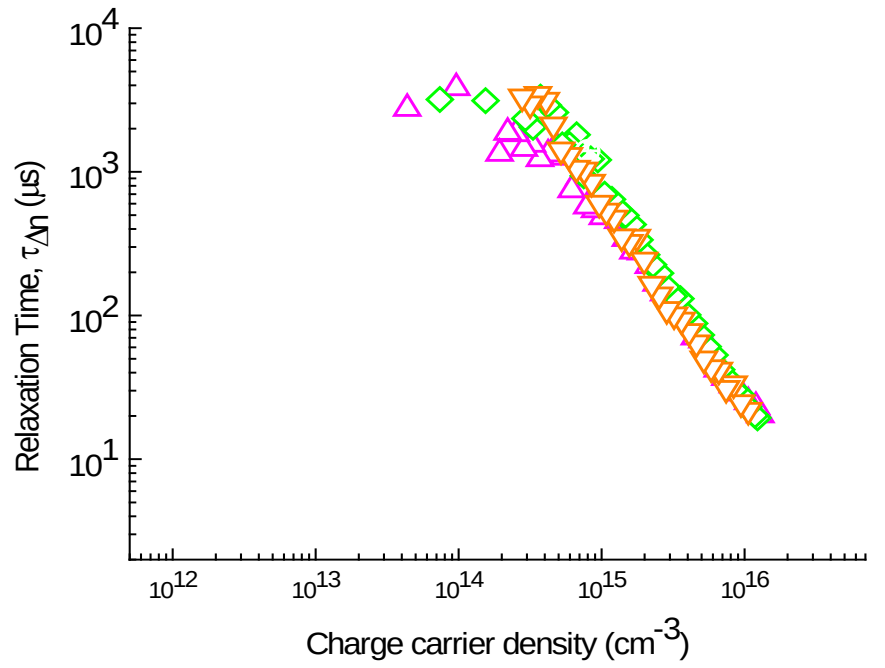

(a)

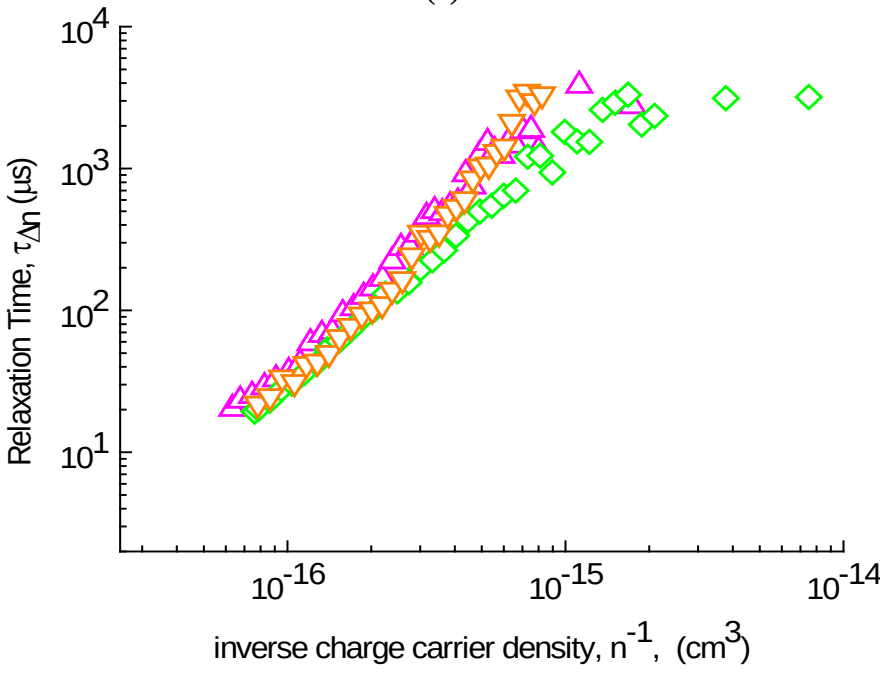

(b)

Figure 4.4. (a) Carrier relaxation time, $\tau_{\Delta n}$, plotted as a function of charge carrier density. (b) plotted as a function of inverse charge carrier density. The (△) represents data from T66-F1, (◇) represents data from T66-F2, and (▽) represents data from T66-F3.

There is much debate about the physical mechanism involved in the relaxation of photo-excited electron-hole pairs in organic photocells. If carrier recombination occurs

through the Langevin mechanism we expect $\tau = \frac{1}{\gamma n}$ and taking the derivative $\left(\frac{d\tau}{d\left(\frac{1}{n}\right)}\right)$ we obtain the $\gamma(n)$ dependence shown in Fig. 4.5. The data is very scattered but there is a clear variation of γ with charge density. This is not anticipated in the Langevin model:

$$\gamma = \frac{q\mu}{\varepsilon\varepsilon_0} \tag{14}$$

Assuming $\mu_e \sim 10^{-3}$ cm^2 V s^{-1}, $\mu_p \sim 10^{-4}$ cm^{2}Vs^{-1} and $\varepsilon \sim 3.4$ we estimate $\gamma \sim 10^{-9}$ s cm^6 which is 10^3 times larger than the maximum observed in Fig. 4.5 ($\sim 10^{-12}$ cm^3 s^{-1}). Similar discrepancies have been pointed out by other authors [5-7]. Murthy et al. [6] have proposed a model leading to a reduced Langevin γ coefficient. In their approach Langevin recombination leads to an intermediary state in which the electrons and holes have reached a state wherein they can either recombine completely or they can, via a back reaction, escape recombination leading to an effective reduction in γ. This effective γ could be applied in all the standard Langevin based equations (Eqs. 4.6 through 4.8) but it would not explain behavior cited above following Eq. 4.9 and shown in Fig. 4.5. Our data confirms that Langevin is probably not the primary mechanism (consistent with Shuttle et al. deductions [2]) but they do not enable us to shed more light onto the issue.

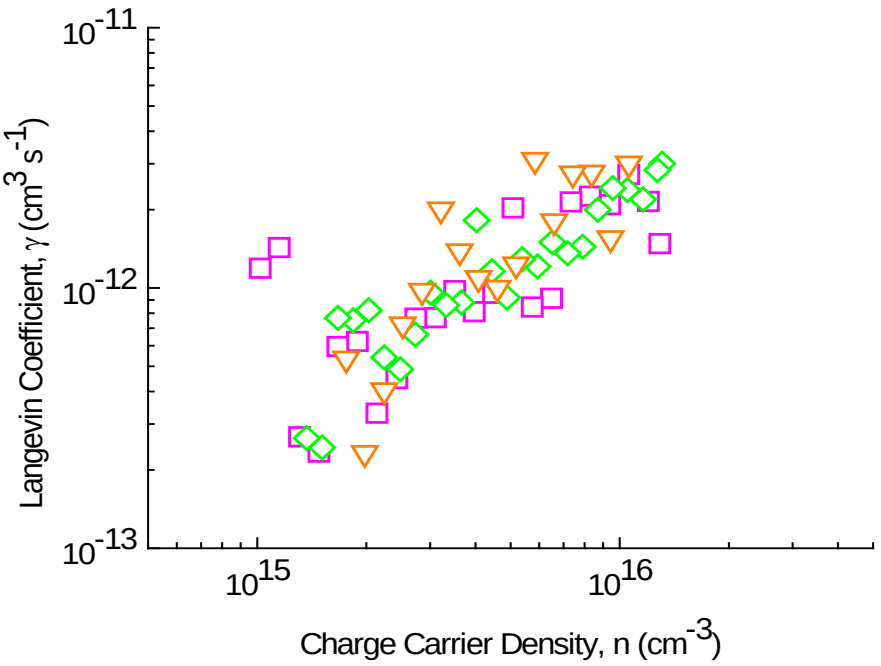

Figure 4.5. The Langevin coefficient, γ, as a function of charge carrier density required to explain the variation of γ(n) observed experimentally. Only data for n > 10^{15} cm^{-3} is presented since $\tau_{\Delta n}$ becomes independent of n below and this is not anticipated by the Langevin model. The (△) represents data from T66-F1, (◇) represents data from T66-F2, and (▽) represents data from T66-F3.

4.1.4 Summary

We have established our own data base for the behavior of unirradiated photocells and determined several facts. In the first instance the transient photovoltaic measurement yields a carrier recombination time which is shorter than the relaxation time determined if one considers the totality of the photocarriers including those generated by the background light level. The difference is a factor of 2.4 in our case. We observe a saturation phenomena in $\tau_{\Delta n}$ versus V_{oc} which occurs for values < 0.3 V. This saturation correlates with the differential capacitance becoming limited by the geometrical capacitance and, combined with a shunt resistance effect is dictated by R_sC_{geom}. Using a Langevin recombination model to explain $\tau_{\Delta n}(V_{oc})$ requires a recombination constant which varies with carrier density – this is inconsistent with the recognized model. If we

force the data to fit the Langevin model we obtain a coefficient which is ~ 10^3 times smaller than anticipated by theory. It remains to be established how irradiation impacts these various parameters.

4.2 Radiation Data

Having explored the case of an unirradiated diode subject to variations in the open circuit voltage induced by changes in the background light level we now examine the results of radiation exposure. In space, in a relatively low Earth orbit, solar cells are primarily subject to energetic electrons and protons which lose energy in the cell by deposition of ionizing energy (see Chapter 1). We therefore "simulate" space using an X ray source which generates ionizing radiation although we note that dose rates will be several orders of magnitude larger than those experienced in space. We present the radiation data in two steps. In the first case we establish a desired V_{oc} by adjusting the background light level and take an initial parameter measurement. Then we begin irradiation to various accumulated doses. After reaching the desired accumulated dose, the x-irradiation is turned off for 1 minute in order to perform the necessary measurements. Though some measurements for radiation doses up to ~ 1200 krads (SiO_2) were performed, the majority of those which will be discussed were in the range 0 – 300 krads(SiO_2). In the second step devices were irradiated to a desired total dose then a full complement of device parameters measured (that is to say, the background light level was adjusted to establish a wide range of V_{oc} values at which a set of measurements was performed) .

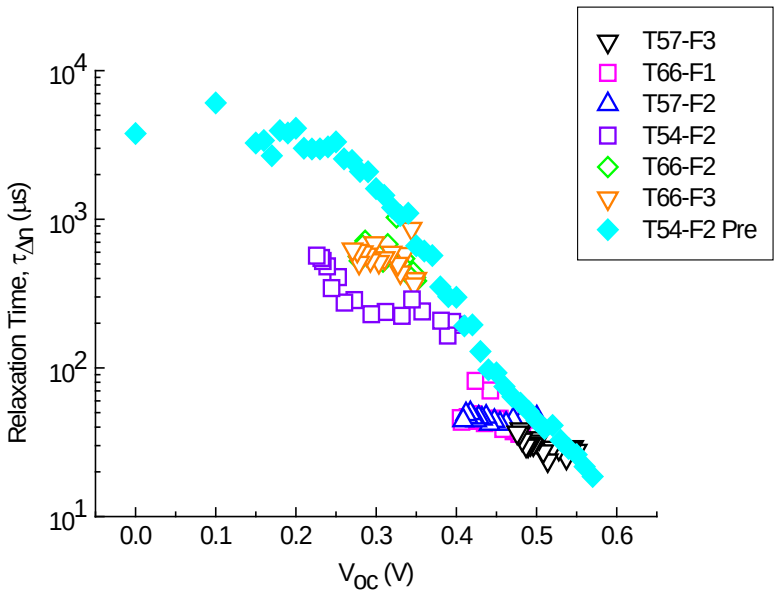

Figure 4.6. Relaxation time as a function of V_{oc} for a variety of radiation experiments. Each data set corresponds to an initial V_{oc} determined by the background light level subjected to irradiation to at least 300 krads(SiO_2). (▽) had a starting background V_{oc} = 0.55V, both (□ , △) had a starting background V_{oc} = 0.50V, (□) had a starting background V_{oc} = 0.40V, both (◇, ▽) had a starting background V_{oc} = 0.35V. The cyan data (◆) shows the behavior observed when changes in $\tau_{\Delta n}$ result solely from variation of the background light level.

4.2.1 Relaxation Time vs V_{oc}

Using the methodology described in the previous chapter and adjusting the pulse intensity so as to best as possible work with small but constant δV_{oc}, we obtained the values of $\tau_{\Delta n}(V_{oc})$ shown in Fig. 4.6 as a function of accumulated radiation dose. To understand this plot, consider the data shown by the violet symbol (□); here we established an initial background V_{oc} of 0.4V. As we irradiated the device, the relaxation time remained initially "constant," but the V_{oc} decreased. This is in contrast to the data

presented in Fig. 4.1 in the un-irradiated case where variation of V_{oc} by adjustment of the background light level clearly induced a variation in $\tau_{\Delta n}$. If this relationship were simple, one would expect that because the V_{oc} is changing with accumulated dose (Fig. 4.7), then the relaxation time would change as well. However, the relaxation time remains constant until ~300 krads(SiO_2) accumulated dose and then begins to increase.

It is also interesting to observe that the relaxation time when starting at higher V_{oc}'s remains constant for larger accumulated doses, this is shown in Fig. 4.6 with the black (▽) blue (△) and magenta (□) data.

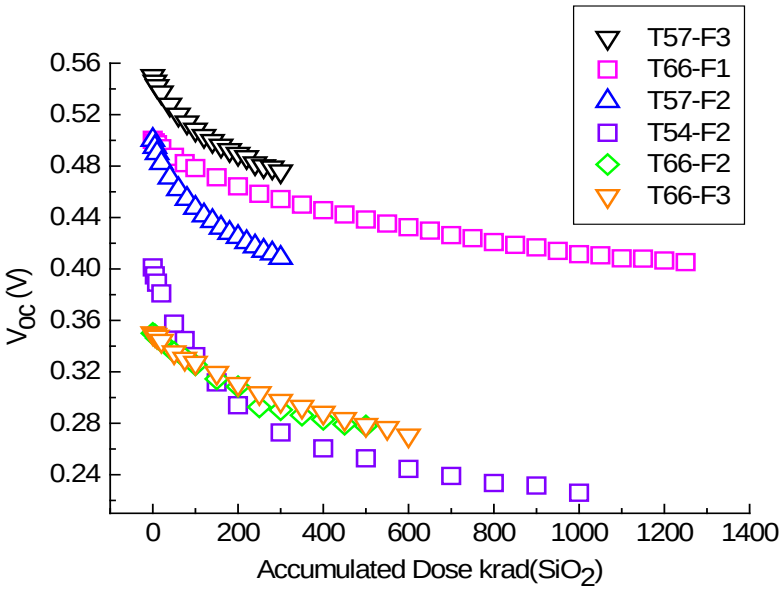

Figure 4.7. V_{oc} versus accumulated dose. Each data set corresponds to an initial V_{oc} determined by the background light level subjected to irradiation to at least 300 krads(SiO_2). (▽) had a starting background V_{oc} = 0.55V, both (□ , △) had a starting background V_{oc} = 0.50V, (□) had a starting background V_{oc} = 0.40V, both (◇, ▽) had a starting background V_{oc} = 0.35V.

The data is also repeated in Fig. 4.8 but here we present the relaxation time as a function of accumulated radiation dose. Examination of the data shown by the violet squares, reveals that there is no change initially with accumulation of radiation until

~300-400 krads(SiO_2) when the relaxation time begins to increase with dose. The question which immediately comes to mind is that given the extensive analysis for the unirradiated cell case what radiation effect can lead to a ΔV_{oc} without resulting in a $\Delta\tau_{\Delta n}$?

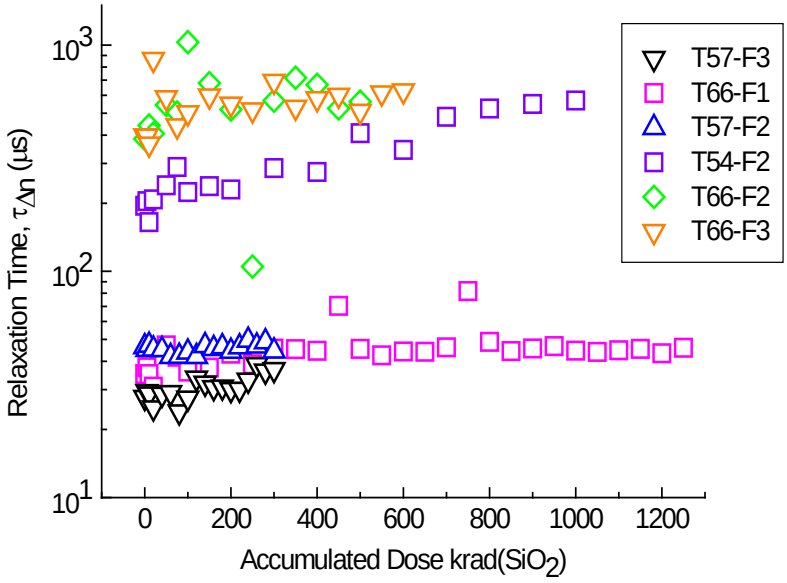

Figure 4.8. Relaxation time as a function of accumulated dose. (▽) had a starting background V_{oc} = 0.55V, both (□ , △) had a starting background V_{oc} = 0.50V, (□) had a starting background V_{oc} = 0.40V, both (◇,▽) had a starting background V_{oc} = 0.35V.

In section 4.1 we discussed the relationship between the relaxation time, $\tau_{\Delta n}$ and the carrier density, n:

$$\frac{d\,\tau_{\Delta n}}{d\,\tau^0_{\Delta n}} = \left(\frac{n_0}{n}\right)^{\lambda} \qquad (15)$$

so that $\tau_{\Delta n} \propto \left(\frac{1}{n}\right)^{\lambda}$. In consequence, invariance of $\tau_{\Delta n}$ is consistent with invariance of the carrier density.

4.2.2 Differential Capacitance vs V_{oc}

We saw previously, with accumulated radiation, the open circuit voltage is decreasing. The differential capacitance, C_{diff}, which is defined as $\frac{dQ}{dV_{oc}}$, also varies with V_{oc} as shown in Fig. 4.9 and as a function of radiation dose as shown in Fig. 4.10. If we examine Fig. 4.9 we see a similar decrease in the differential capacitance with radiation induced V_{oc} as there was in the pre-irradiation case, Fig. 4.2 with background light variation.

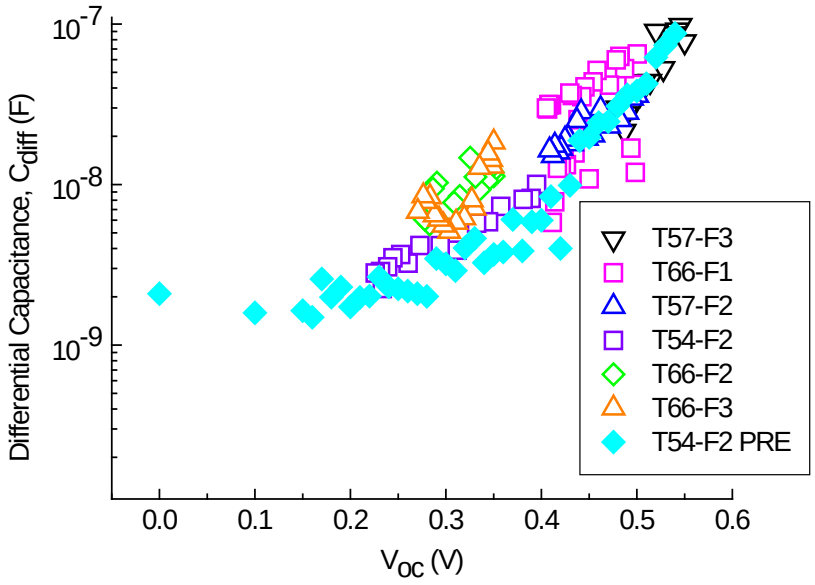

Figure 4.9. Capacitance as a function of open circuit voltage for a variety of accumulated dosages. (▽) had a starting background V_{oc} = 0.55V, both (□, △) had a starting background V_{oc} = 0.50V, (□) had a starting background V_{oc} = 0.40V, both (◇, ▽) had a starting background V_{oc} = 0.35V. The cyan data (◆) shows the behavior observed when changes in $\tau_{□ln}$ result solely from variation of the background light level.

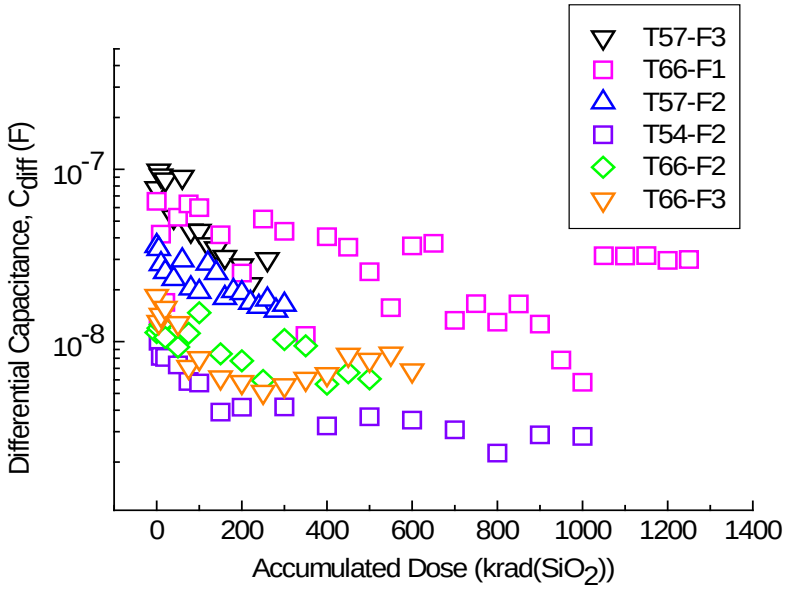

Figure 4.10. Capacitance as a function of accumulated dose. (▽) had a starting background V_{oc} = 0.55V, both (□ , △) had a starting background V_{oc} = 0.50V, (□) had a starting background V_{oc} = 0.40V, both (◇, ▽) had a starting background V_{oc} = 0.35V.

4.2.3 Charge Carrier Density (n) vs V_{oc}

The way we extract the charge carrier density, n, has been outlined in chapter 3 and is based upon determination of the differential capacitance and application of Eq. 4.11. This equation works for the un-irradiated case, but does it work for the radiation case? The results shown in Fig. 4.11 indicate that the analysis that was performed in the un-irradiated case works approximately for the radiation case. The explanation we have put forward is as follows: Consider the initial radiation accumulated dosage < 300 krads(SiO_2), where the measured relaxation time remains constant, but the V_{oc} is decreasing. Because of Figs. 4.9 and 4.10 and the analysis used in the pre-irradiation case using Eq. 4.11, one expects there to be a decrease in n, which would match with charge and the capacitance.

$$n(V_{oc}) = \frac{1}{Aqd}\int_0^{V_{oc}} C_{diff}\, dV \qquad (16)$$

The equation given by Koster et al [3] Eq. 4.12 links the open circuit voltage to the energy gap, E_{gap}, and the photo-induced carrier density, np:

$$V_{oc} = \frac{E_{gap}}{q} - \frac{kT}{q}\ln(\frac{N_c^2}{np}) \qquad (17)$$

Although it was strictly developed for the case of Langevin recombination we examine its predictions for the case of relaxation and V_{oc}. Since N_c is a constant and if np is constant (since the relaxation time is constant in our experiments) V_{oc} must vary without change in carrier density and therefore without change in the relaxation time, τ_n. To allow for this possibility in Eq. 4.12 above, the V_{oc} limit in the integral must be the un-modified one i.e. the value prior to irradiation. We demonstrate this in Fig. 4.11 where we include the n(V_{oc}) values calculated assuming constant carrier density for an initial V_{oc} and where we assume the initial n varies with the measured background V_{oc} value. We postulate that the variations in V_{oc} resulting from irradiation are in fact due to effective changes in E_{gap}.

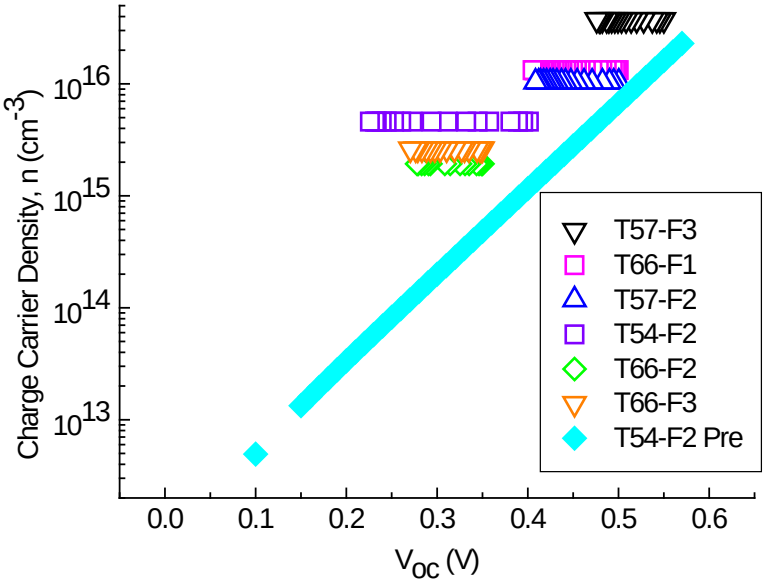

Figure 4.11. Charge carrier density as a function of open circuit voltage for a variety of accumulated radiation doses. (▽) had a starting background V_{oc} = 0.55V, both (□ , △) had a starting background V_{oc} = 0.50V, (□) had a starting background V_{oc} = 0.40V, both (◇, ▽) had a starting background V_{oc} = 0.35V. The cyan symbols (◆) show the charge carrier densities as a function of V_{oc} prior to irradiation.

4.2.4 I_{sc} vs V_{oc} – Supporting Evidence

The short circuit current, I_{sc}, in a photocell of ideality factor , n', and reverse bias saturation dark current, I_o, can be written:

$$1 + \frac{I_{sc}}{I_0} = e^{\frac{qV_{oc}}{n'kT}} \tag{18}$$

So that for $I_{sc}/I_o >> 1$:

$$\ln(I_{sc}) = \ln(I_0) + \frac{qV_{oc}}{n'kT} \tag{19}$$

In Fig. 4.12 we plot I_{sc} versus V_{oc} for the irradiated samples and, shown by the solid squares, the data for unirradiated samples where changes in V_{oc} are due to changes in background light level. To first order the irradiated cells show plateau in $I_{sc}(V_{oc})$ which would correspond the constancy of the photo-generated carrier density for a given

initial V_{oc} value. This conclusion supports the argument put forward for the invariance of the relaxation time discussed above. Similar reasoning applies to the plots of I_{sc}(accumulated dose) shown in Fig. 4.13.

The theoretical value is q/kT = 38.6 eV^{-1} at room temperature. We therefore anticipate a plot of ln(I_{sc}) versus V_{oc} to be a straight line. Such a relationship was indeed found by Potscavage et al. [8] over a limited range of V_{oc} (0.35 – 0.59 V) but with our measured value equal to 29.04 eV^{-1}.

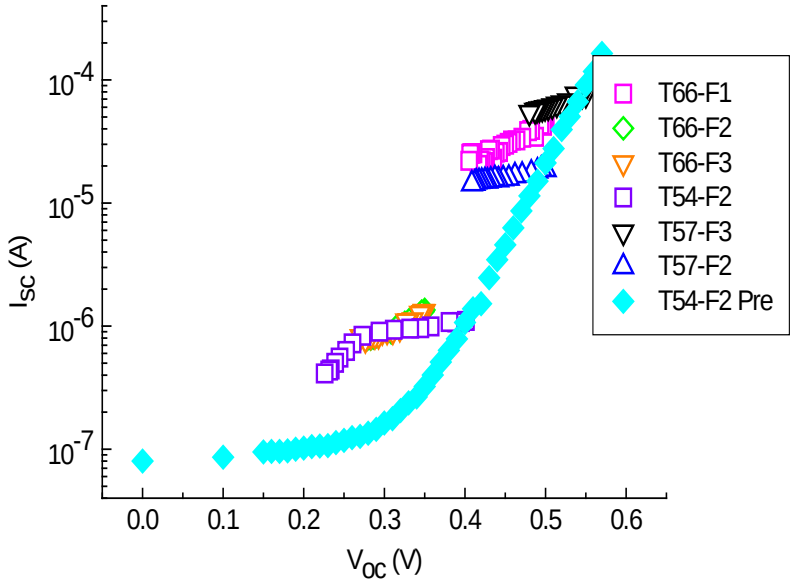

Figure 4.12. Current as a function of open circuit voltage for a variety of accumulated dosages. (▽) had a starting background V_{oc} = 0.55V, both (□ , △) had a starting background V_{oc} = 0.50V, (□) had a starting background V_{oc} = 0.40V, both (◇, ▽) had a starting background V_{oc} = 0.35V. The cyan symbols (◆) show the charge carrier densities as a function of V_{oc} prior to irradiation.

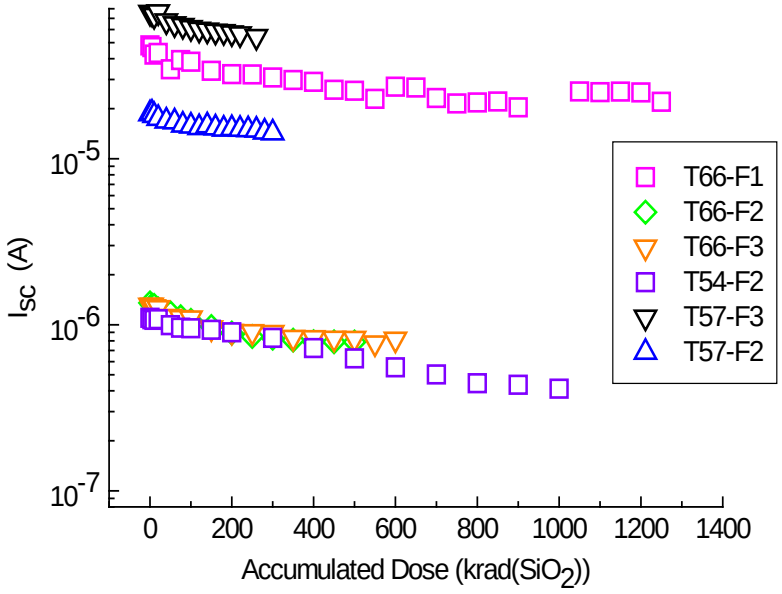

Figure 34.13. Current as a function of accumulated dose. (▽) had a starting background V_{oc} = 0.55V, both (□ , △) had a starting background V_{oc} = 0.50V, (□) had a starting background V_{oc} = 0.40V, both (◇, ▽) had a starting background V_{oc} = 0.35V.

4.3 Post Radiation Data

The data presented in this section is the post irradiation case. That is to say, we perform the pre-irradiation measurements, adjust the background light level to establish a V_{oc} value then irradiate and finally repeat the measurement of $\tau_{\Delta n}$, etc. following adjustment of V_{oc} via the light level.

4.3.1 Relaxation Time vs V_{oc}

The post irradiation measurement of the relaxation time was performed in an analogous manner to the pre-irradiation sweep with the results shown in Fig. 4.14. We notice that post radiation, the relaxation time saturation regime is shorter with V_{oc}. Based on the explanation given for the un-irradiated case, the shunt resistance must be still the

limiting factor at low V_{oc} together with the geometrical diode capacitance forming an RC time constant limit.

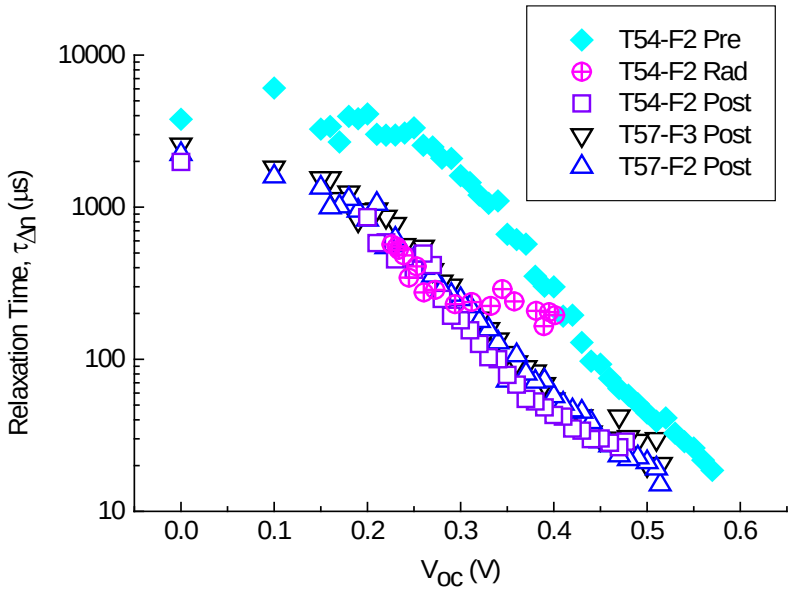

Figure 4.14. Relaxation time as a function of open circuit voltage. (◆) had a starting background is the pre-irradiation data on one of the samples, (⊕) is the radiation data, (□) is the post irradiation sweep after 1000 krads(SiO_2) with initial background V_{oc} = 0.40V, and (▽)is the post irradiation sweep after 300 krads(SiO_2) with initial background V_{oc} = 0.55V. (△) is the post irradiation sweep after 300 krads(SiO_2) with initial background V_{oc} = 0.50V. Note: the naming of these devices are defined as the device sample (T66) followed by the finger on that sample (-F1).

4.3.2 Differential Capacitance vs V_{oc}

The results in Fig. 4.15 show that the maximum capacitance levels have decreased with accumulation of radiation. The capacitance level follows the open circuit voltage decrease given in the explanation in the radiation section of this chapter.

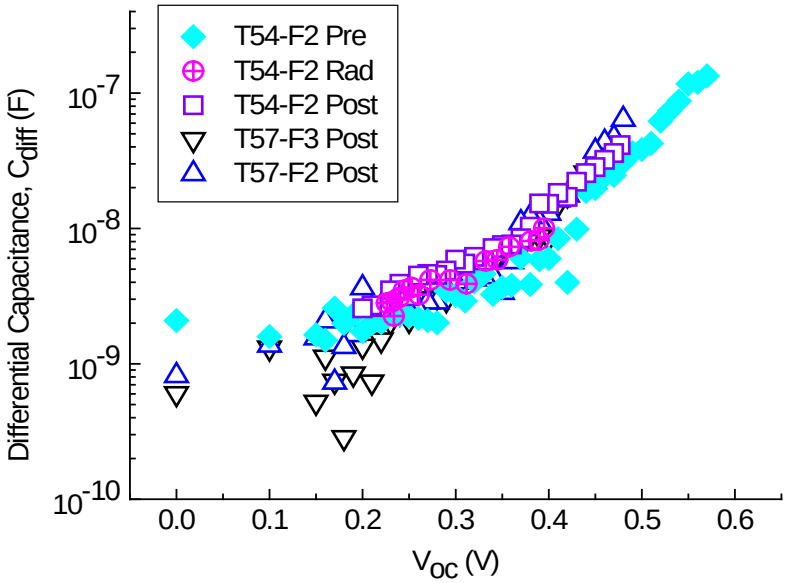

Figure 4.15. Capacitance as a function of open circuit voltage. (◆) had a starting background is the pre-irradiation data on one of the samples, (⊕) is the radiation data, (□) is the post irradiation sweep after 1000 krads(SiO_2) with initial background V_{oc} = 0.40V, and (▽)is the post irradiation sweep after 300 krads(SiO_2) with initial background V_{oc} = 0.55V. (△) is the post irradiation sweep after 300 krads(SiO_2) with initial background V_{oc} = 0.50V.

4.3.3 Charge Carrier Density vs V_{oc}

The charge carrier density slope changes after an accumulated dose of radiation compared with the pre-irradiation case. Though the data is very scattered we see that for a chosen constant value of n there is a corresponding δV_{oc} between the unirradiated and irradiated cases indicating that there is a scenario possible in which radiation induces a change in V_{oc} leaving n essentially constant.

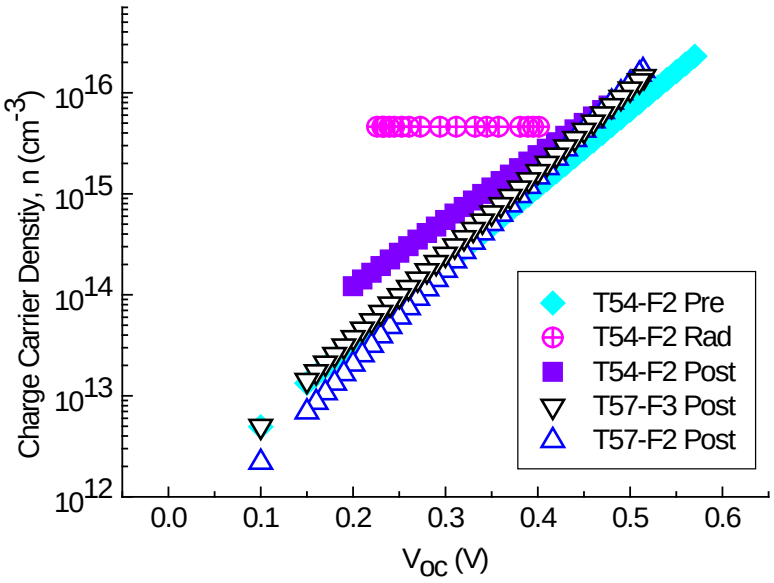

Figure 4.16. Charge carrier density as a function of open circuit voltage. (◆) had a starting background is the pre-irradiation data on one of the samples, (⊕) is the radiation data, (□) is the post irradiation sweep after 1000 krads(SiO_2) with initial background V_{oc} = 0.40V, and (▽)is the post irradiation sweep after 300 krads(SiO_2) with initial background V_{oc} = 0.55V. (△) is the post irradiation sweep after 300 krads(SiO_2) with initial background V_{oc} = 0.50V.

4.3.4 Current vs V_{oc}

The data shown in Fig. 4.17 is consistent with the argument that radiation essentially shifts the unirradiated curve to lower V_{oc} whilst maintaining n essentially constant, hence constant $\tau_{\Delta n}$ as measured.

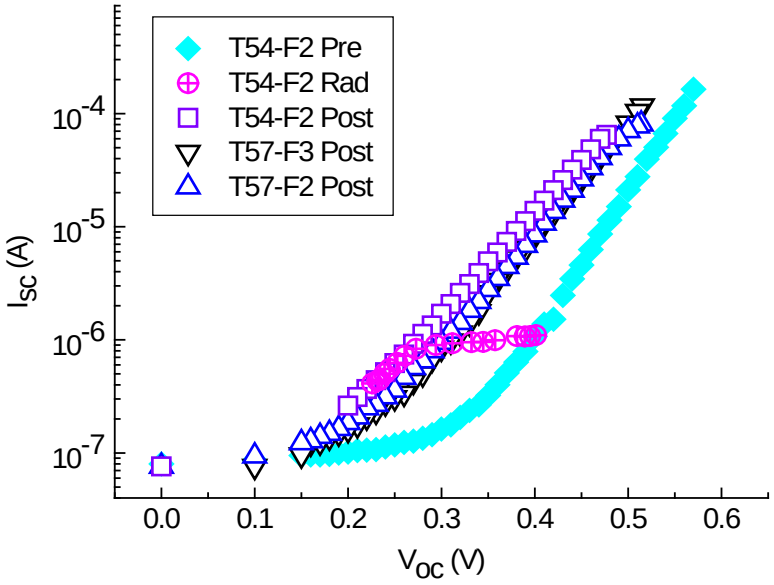

Figure 4.17. Short circuit current as a function of open circuit voltage. (◆) had a starting background is the pre-irradiation data on one of the samples, (⊕) is the radiation data, (□) is the post irradiation sweep after 1000 krads(SiO_2) with initial background V_{oc} = 0.40V, and (▽)is the post irradiation sweep after 300 krads(SiO_2) with initial background V_{oc} = 0.55V. (△) is the post irradiation sweep after 300 krads(SiO_2) with initial background V_{oc} = 0.50V.

4.3.5 Summary

The primary effect of irradiation on the cell characteristics is to decrease the apparent open circuit voltage, V_{oc}, without change in the photoinduced charge carrier relaxation time, $\tau_{\Delta n}$. Given the expected relationship between $\tau_{\Delta n}$ and V_{oc} [3] this is surprising. However, data on the carrier density as a function of irradiation suggests this may change little which would be consistent with the invariance of $\tau_{\Delta n}$. This conclusion implies that radiation modifies the effective V_{oc} independent of the charge density.

4.4 References for Chapter 4

[1] C. Kouhestani, K. Kambour, D. Nguyen, C. Mayberry, R. A. B. Devine, C-C. Chen, G. Li and Y. Yang, “Mechanism of Carrier Relaxation in Unirradiated P3HT:PCBM Organic Photo-Cells I. Experiment,” (to be published) 2014.

[2] Shuttle, C. G., O'Regan, B., Ballantyne, A. M., Nelson, J., Bradsley, D. D. C., De Mello, J., & Durrant, J. R. (2008). Experimental determination of the rate law for charge carrier decay in a polythiophene: Fullerene solar cell. *Applied Physics Letters*, *92*(9), 3311.

[3] Koster, L. J. A., Mihailetchi, V. D., Ramaker, R., & Blom, P. W. M. (2005). Light intensity dependence of open-circuit voltage of polymer: fullerene solar cells. *Applied Physics Letters*, *86*(12), 123509-123509.

[4] K. Kambour, C. Kouhestani, D. Nguyen, C. Mayberry, R. A. B. Devine, C-C. Chen, G. Li and Y. Yang, “Mechanism of Carrier Relaxation in Unirradiated P3HT:PCBM Organic Photo-Cells II. Modelling,” (to be published) 2014

[5] Foertig, A. (2013). Recombination Dynamics in Organic Solar Cells. Wurtzburg University

[6] D. H. K. Murthy, A. Malianas, Zheng Tang, G. Juska, K. Arlauskas, F. Zhang, D. A. Siebbeles, O. Inganas and T. J. Savenije, “Origin of bimolecular recombination in blends of conjugated polymers and fullerenes”, Adv. Funct. Mater. 34 (23) 4262-4268 (2013)

[7] Rauh, D., Deibel, C., & Dyakonov, V. (2012). Charge density dependent nongeminate recombination in organic bulk heterojunction solar cells. Advanced Functional Materials, 22(16), 3371-3377.

[8] Potscavage Jr, W. J., Sharma, A., & Kippelen, B. (2009). Critical interfaces in organic solar cells and their influence on the open-circuit voltage. *Accounts of chemical research*, *42*(11), 1758-1767.

5 Chapter 5 – Conclusion

5.1 Summary of Work

The initial objective of the work presented in this thesis was to examine how ionizing radiation would impact the performance of organic semiconductor based photo-voltaic cells such as those manufactured using P3HT:PCBM blends. It became rapidly obvious that before performing such research, in-depth studies of the unirradiated cells were essential. In particular a question yet unanswered in the literature concerned the primary mechanism of recombination of photo-excited electrons and holes. For these reasons the experimental data sections in Chapter 4 are heavily weighted towards understanding the basic physics of cell photo-response and the radiation data is somewhat preliminary. The results of the experiments described led to a series of conclusions which are important for our ultimate goal; understanding the effects of ionizing radiation. In particular the results of the study lead us to conclude:

- From the differential capacitance measurement as a function of V_{oc} we find values for q/2kT which are seriously inconsistent with the value 19.3 eV^{-1} expected on the basis of pure Langevin recombination [1].
- The Langevin constant γ is at least three orders of magnitude smaller than the theoretical value calculated from known parameters such as the dielectric constant and carrier mobilities [1].

- The Langevin coefficient determined appears to be charge carrier density dependent.
- $\tau_{\Delta n}$ variation for $V_{oc} < 0.3$ V is determined by the RC time constant behavior of the photo-diode and is not evidence for the onset of another relaxation mechanism such as monomolecular relaxation [1] as has been suggested by various authors.
- The work presented shows that not only will organic photovoltaics survive in a space environment; they will thrive contrary to popular belief.
- The initial effect of radiation is to accumulate charge in the PEDOT:PSS anode material.
- For doses of accumulated radiation krads(SiO_2)) the only characteristics that appear to be changing are the open circuit voltage and the band gap energy - this is required to explain the constant relaxation time ($\tau_{\Delta n}$) and charge carrier density (n).In the turn up region of $\tau_{\Delta n}$ with the increase of accumulated radiation, we believe that another mechanism is changing as well to cause the open circuit voltage and the effective band gap energy to change the all of the measured parameters (τ, C, n, I).

- These issues will be addressed further in the future work dealing with modelling of the photo-response using commercially available codes.

5.2 Future work

There are still a lot of questions that need to be answered which translate into a significant volume of work that needs to be done in the understanding these organic photovoltaics.

Some of the work that I would have liked to have done was to study the influence of the morphology of the active layer. This may be a crucial part in understanding what happens subsequently in the space environment. For example, what are the electrical and physical characteristics during each stage of the fabrication process? What happens to these characteristics during radiation? What about immediately after irradiation? Does the device anneal differently as a function of the blend morphology? A useful way to determine this is through a combination of IMPS (Intensity modulated photocurrent spectroscopy) and RAMAN spectroscopy [2, 3].

Another experiment that I would have liked to have performed concerns the mobility measurement [4]. We have used mobilities that are found in literature [5], but it would be interesting to determine if there is a morphology dependence, radiation dependence, etc. With these solar devices being a blend material, what is the variability of the mobility with different devices?

Some of the further analysis I would have liked to have performed involves measurement of the annealing of radiation effects, if there are any. Does the device anneal after radiation is accumulated? If so, what characteristics change? Why do they anneal? How much do they anneal? How long does it take to anneal before it saturates? Do they anneal back to their pre-irradiation values?

Other measurements that need to be taken are longer radiation runs for the high background V_{oc} experiments to determine if there is ever a turn up region in $\tau_{\Delta n}$ and where that would be.

The end goal would eventually try to link a specific mechanism to the conversion efficiency. Once this has been achieved, we can begin fabrication of these devices with

this in mind in order to maximize the conversion efficiency, minimize fabrication cost, and material utilization.

With the radiation experiments that have been performed in this text, we only used X-irradiation to obtain high ionizing radiation doses quickly. We have not made the measurements that simulate a specific space environment that irradiate at low accumulation dose rates. The next thing to do is to retake all of these measurements with different materials other than P3HT:PCBM of equal or higher power conversion efficiencies and compare them to determine if the fundamental physics of degradation is the same [6]. Do the different materials exhibit similar behavior in each of these measurements? If not, why?

Finally it would be desirable to model the cell behavior using commercially available code [7] and thus open up an alternative route to predicting device performance prior to performing experiments.

5.3 References for Chapter 5

[1] C. Kouhestani, K. Kambour, D. Nguyen, C. Mayberry, R. A. B. Devine, C-C. Chen, G. Li and Y. Yang, "Mechanism of Carrier Relaxation in Unirradiated P3HT:PCBM Organic Photo-Cells I. Experiment," (to be published) 2014.

[2] Ponomarev, E. A., & Peter, L. M. (1995). A generalized theory of intensity modulated photocurrent spectroscopy (IMPS). *Journal of Electroanalytical Chemistry*, *396*(1), 219-226.

[3] Cheung, D. L., & Troisi, A. (2010). Theoretical Study of the Organic Photovoltaic Electron Acceptor PCBM: Morphology, Electronic Structure, and Charge Localization†. *The Journal of Physical Chemistry C*, *114*(48), 20479-20488.

[4] Sconza, A., & Torzo, G. (1987). A simple and instructive version of the Haynes-Shockley experiment. *European Journal of Physics*, *8*(1), 34.

[5] Vanlaeke, P., Swinnen, A., Haeldermans, I., Vanhoyland, G., Aernouts, T., Cheyns, D., ... & Manca, J. V. (2006). P3HT/PCBM bulk heterojunction solar cells: Relation between morphology and electro-optical characteristics. *Solar Energy Materials and Solar Cells*, *90*(14), 2150-2158.

[6] Hou, J., & Guo, X. (2013). Active Layer Materials for Organic Solar Cells. In *Organic Solar Cells* (pp. 17-42). Springer London.

[7] K. Kambour, C. Kouhestani, D. Nguyen, C. Mayberry, R. A. B. Devine, C-C. Chen, G. Li and Y. Yang, "Mechanism of Carrier Relaxation in Unirradiated P3HT:PCBM Organic Photo-Cells II. Modelling," (to be published) 2014